A phase field model of unsaturated flow

A phase field model of unsaturated flow

L. Cueto-Felgueroso[1] and R. Juanes[1]

Received 7 March 2009; revised 4 June 2009; accepted 30 June 2009; published 7 October 2009.

[1] We present a phase field model of infiltration that explains the formation of gravity fingers during water infiltration in soil. The model is an extension of the traditional Richards equation, and it introduces a new term, a fourth-order derivative in space, but not a new parameter. We propose a scaling that links the magnitude of the new term to the relative strength of gravity-to-capillary forces already present in Richards' equation. We exploit the thermodynamic framework to design a flow potential that constrains the water saturation to be between 0 and 1, its physically admissible values. The model predicts a saturation overshoot at the wetting front, which is in good agreement with experimental measurements. Two-dimensional numerical simulations predict gravity fingers with the appearance and characteristics observed in visual laboratory experiments. A linear stability analysis of the model shows that there is a direct relation between saturation overshoot and the strength of the front instability. Therefore our theory supports the conjecture that saturation overshoot, a pileup of water at the wetting front, is a prerequisite for gravity fingering.

Citation: Cueto-Felgueroso, L., and R. Juanes (2009), A phase field model of unsaturated flow, *Water Resour. Res.*, *45*, W10409, doi:10.1029/2009WR007945.

1. Introduction

[2] Infiltration of water in soil is an essential component of the hydrologic cycle [*Horton*, 1933; *Hillel*, 1980; *Domenico and Schwartz*, 1998]. It governs the presence of water and life at the land-atmosphere interface, in particular soil moisture [*Liang et al.*, 1994] and vegetation [*Rodriguez-Iturbe et al.*, 1999]. It also controls seasonal aquifer recharge in arid regions [*Allison et al.*, 1994; *Sophocleous*, 2002], and soil weathering at the scale of millennia [*Torn et al.*, 1997; *Markewitz et al.*, 2001]. All of these feedbacks will be even more important under a scenario of global climate warming [*Porporato et al.*, 2004], and will likely become crucial in an assessment of global desertification [*Schlesinger et al.*, 1990].

[3] Infiltration is modeled using a variety of approaches, depending on the scale (and scope) of the problem [*Philip*, 1969; *Hillel*, 1980]. These range from the Horton method [*Horton*, 1940; *Philip*, 1957] and the Green-Ampt approximation [*Green and Ampt*, 1911; *Philip*, 1957], to the solution of Richards' equation [*Richards*, 1931]: a partial differential equation that describes the evolution of water content in space and time, which is based on conservation of mass and the Darcy-Buckingham equation of fluid flux in an unsaturated medium [*Buckingham*, 1907].

[4] Richards' equation, however, is unable to explain why the infiltration of water in homogeneous dry soil displays preferential flow, in the form of "fingers" [*Hill and Parlange*, 1972; *Raats*, 1973]. In one dimension, it is also unable to explain the common experimental observation that the water pressure [*Stonestrom and Akstin*, 1994; *Geiger and Durnford*, 2000] and water saturation [*DiCarlo*, 2004; *Shiozawa and Fujimaki*, 2004] is higher at the wetting front than behind the front. These two phenomena (saturation overshoot and gravity fingering) are believed to be inextricably linked [*Geiger and Durnford*, 2000; *Eliassi and Glass*, 2001], and this is confirmed by experimental evidence [*DiCarlo*, 2004]. Experiments show that pressure overshoot is not sufficient for the development of the instability, but saturation overshoot is [*DiCarlo*, 2007]. Previous work has also shown, from the linear stability analysis of a dynamic capillary pressure model, that the degree of nonmonotonicity is related to the severity of the instability [*Egorov et al.*, 2003; *Nieber et al.*, 2005].

[5] Recently, we put forward the fundamental idea of including the effect of a macroscopic interface (the wetting front) in the mathematical description of unsaturated flow [*Cueto-Felgueroso and Juanes*, 2008]. This was done following a phase field approach, where a gradient term in the energy appears naturally, leading to a fourth-order term in the mass conservation equation. The model predicts gravity fingering, and the results of the linear stability analysis agree well with the experiments of *Glass et al.* [1989b] in terms of finger width and finger velocity. The inspiration for the new model is the flow of thin films (like water down a plane), which also displays fingering instability [*Huppert*, 1982]. We then cast the model in the rigorous framework of phase field models and nonlocal thermodynamics [*Cahn and Hilliard*, 1958].

[6] This paper builds on that idea. We extend the model, exploiting the power of the phase field methodology, to constrain the saturations between 0 and 1, clearly a physical requirement. We compare extensively with experiments of saturation overshoot [*DiCarlo*, 2004], and find good agreement between model predictions and lab measurements, not only in terms of saturation overshoot but also for the entire

[1]Department of Civil and Environmental Engineering, Massachusetts Institute of Technology, Cambridge, Massachusetts, USA.

0043-1397/09/2009WR007945$09.00

nonmonotonic saturation profile. We investigate the impact of mild heterogeneity in two-dimensional simulations, and find that the preferential flow pattern is preserved, leading to realistic simulations of gravity fingering. We also analyze (and confirm) that saturation overshoot is indeed a prerequisite for finger formation. From the linear stability analysis, we find that there is a direct correspondence between the magnitude of the overshoot and the severity of the instability. We explain the derivation of the complete model, we give the physical reasoning behind it, and we frame it in the context of the entire body of literature on unstable unsaturated flow.

[7] The new model is appealing. It is a simple extension of Richards' equation, with a new term but without a new parameter. It reproduces the two key features of unsaturated flow: a nonmonotonic saturation profile, and the formation and persistence of gravity fingers. It shows good quantitative agreement with experiments in terms of tip saturation, tip velocity and finger width. The most attractive aspect is, however, that the new model offers a starting point for fundamentally new formulations of multiphase flow in porous media.

[8] It is well known that hysteresis alone (without saturation overshoot) cannot explain fingering [*Eliassi and Glass*, 2001; *van Duijn et al.*, 2004; *Nieber et al.*, 2005; *Fürst et al.*, 2009]. In this paper we show that our model can explain the features of fingered flow, including the saturation behind the front, without resorting to hysteresis, thereby resulting in a much simpler mathematical model. We do not argue, however, that hysteresis is unimportant. Hysteresis is a very real phenomenon, with important macroscopic consequences [*Liu et al.*, 1994; *Bauters et al.*, 1998; *Spiteri and Juanes*, 2006; *Juanes et al.*, 2006]. It is likely that agreement with experimental data can be improved with hysteretic capillary pressure and relative permeability functions, and this can be incorporated readily in our model. The proposed model is for unsaturated flow, and it is no longer valid under fully saturated conditions. Extending the model to saturated-unsaturated conditions is not trivial.

[9] We hope the model will be tested against more experimental data, to probe its range of applicability. One of the most interesting aspects is likely to be the strength of the new term. While we have good reasons to defend the proposed scaling (it allowed us to explain finger width, finger velocity, saturation overshoot, and the length of the traveling wave, without resorting to any tuning of the strength of the new term), its widespread validity remains to be investigated.

[10] In section 2 we review infiltration experiments and existing models of unsaturated flow, highlighting their departure from Richards' equation. In section 3 we give a brief overview of the mathematical model of flow of thin films, and stability characteristics of such flows. In section 4 we introduce the essential aspects of phase field models of interface dynamics. Next, in section 5, we present the proposed model of infiltration. We motivate it by means of the thin-film equation, and then formalize it within the framework of phase field models. In section 6 we present numerical simulations of 1-D and 2-D systems. In section 7 we give a summary of the linear stability analysis, which explains the relation between saturation overshoot and gravity fingering. We finish the paper with some conclusions and an outlook.

2. Infiltration Experiments and Existing Models of Unsaturated Flow

2.1. Experimental Evidence of Gravity Fingering

[11] Experiments of water infiltration into dry, homogeneous sand, pervasively show preferential flow, in the form of "gravity fingers." Experimental and theoretical work was initiated in the 1970s [*Hill and Parlange*, 1972; *Philip*, 1975; *Parlange and Hill*, 1976]. Since then, carefully designed experiments have repeatedly shown gravity fingering during infiltration in homogeneous sands [*Diment and Watson*, 1985; *Glass et al.*, 1989b; *Selker et al.*, 1992a; *Lu et al.*, 1994; *Bauters et al.*, 2000; *Yao and Hendrickx*, 2001; *Sililo and Tellam*, 2000; *Wang et al.*, 2004]. The selected pattern of the phenomenon is a winner-takes-all process, in which the fastest growing fingers channelize most of the flow, and the growth of other incipient fingers is thereby suppressed [*Glass et al.*, 1989b; *Selker et al.*, 1992b]. The fully formed fingers advance as traveling waves (with constant shape and velocity), and a saturation overshoot is observed at the tip of the fingers [*Selker et al.*, 1992b; *DiCarlo*, 2004]. The initial moisture content plays a critical role in the fingering instability: even relatively low saturations lead to a compact, downward moving wetting front [*Lu et al.*, 1994; *Bauters et al.*, 2000]. Stable fronts are also observed in dry media when the infiltration rate is either very small or approaches the saturated conductivity [*Hendrickx and Yao*, 1996]. In general, larger infiltration rates produce faster, thicker fingers [*Glass et al.*, 1989b].

[12] Many authors have approached the wetting front instability by drawing an analogy with the two-fluid system in a Hele-Shaw cell [*Saffman and Taylor*, 1958], and their analyses have led to kinematic models that reproduce trends observed in the experiments, such as relations between finger width and finger tip velocity with the flow rate through the finger [*Chuoke et al.*, 1959; *Weitz et al.*, 1987; *Parlange and Hill*, 1976; *Glass et al.*, 1989a; *Selker et al.*, 1992b; *DiCarlo and Blunt*, 2000].

[13] Given that a saturation overshoot occurs at the tip of the fingers, recent experimental work has focused on reproducing this phenomenon in one-dimensional experiments [*Stonestrom and Akstin*, 1994; *Geiger and Durnford*, 2000; *DiCarlo*, 2004; *Shiozawa and Fujimaki*, 2004; *DiCarlo*, 2007]. In fact, it is widely believed that accumulation of water at the wetting front is a prerequisite for triggering the fingering instability [*Geiger and Durnford*, 2000; *Eliassi and Glass*, 2001; *Egorov et al.*, 2003]. These experiments have shown conclusively that there is a critical initial saturation above which the saturation profile is monotonic [*Lu et al.*, 1994; *Bauters et al.*, 2000; *Shiozawa and Fujimaki*, 2004; *DiCarlo*, 2004, 2007]. They have also elucidated the role of the infiltration flow rate: the saturation overshoot increases with increasing flow rate up to a certain value, beyond which it decreases until the overshoot disappears completely under fully saturated infiltration conditions [*DiCarlo*, 2004].

2.2. Pore-Scale Models

[14] Numerical models that implement the fluid-fluid displacement mechanisms have been successful at reproduc-

ing the regime transitions among viscous fingering, capillary fingering and stable displacement observed experimentally [*Lenormand et al.*, 1988]. This can be achieved by means of modified invasion-percolation algorithms that incorporate the dynamics of fluid displacement [*Blunt et al.*, 1992; *Avraam and Payatakes*, 1995; *Lee et al.*, 1996; *Valavanides et al.*, 1998; *Yortsos et al.*, 1997; *Aker et al.*, 1998; *Dahle and Celia*, 1999; *Ferer et al.*, 2004].

[15] The effect of gravity on capillary-dominated displacements can be stabilizing [*Birovljev et al.*, 1991] or destabilizing [*Frette et al.*, 1992]. Gravity affects the structures that form in two-phase flow through correlated buoyancy [*Auradou et al.*, 1999]. Extensions to the modified invasion-percolation models at the pore scale have, indeed, permitted simulating unstable gravity flows [*Onody et al.*, 1995; *Glass and Yarrington*, 1996, 2003; *Zhang et al.*, 2000]. They have been used to propose extensions to Lenormand's phase diagram [*Lenormand et al.*, 1988] in order to account for gravity forces [*Lee et al.*, 1996; *Ewing and Berkowitz*, 1998; *Berkowitz and Ewing*, 1998], and have led to the analysis of the roughening of drainage fronts under combined viscous, capillary, and gravity forces [*Méheust et al.*, 2002].

2.3. Continuum Models

[16] Despite the abundant experimental evidence, the description of unstable gravity-driven unsaturated flow using macroscopic mathematical models (continuum balance laws) has remained a formidably challenging task.

[17] Unsaturated flow is traditionally modeled at the continuum scale using Richards' equation [*Richards*, 1931], which we express in several space dimensions as follows:

$$\phi \frac{\partial S}{\partial t} + \nabla \cdot [K_s k_r(S)(\nabla z + \nabla \psi(S))] = 0, \qquad (1)$$

where S [−] is the water saturation, ϕ [−] is the porosity, K_s [LT^{-1}] is the saturated hydraulic conductivity, and z [L] is depth (coordinate in the direction of gravity). The equation involves two functions of saturation: the relative permeability to water, k_r [−], and the suction head (or capillary pressure in units of head), ψ [L]. The relative permeability is typically a monotonically increasing and convex function of saturation. The capillary pressure is a monotonically decreasing function of saturation and often has one inflection point. Both properties display strong hysteresis effects [*Bear*, 1972; *Dullien*, 1991].

[18] Richards' equation is a statement of conservation of mass together with several assumptions, including: the medium remains unsaturated (S strictly less than 1); the mobility and compressibility of air are much larger than those of water; and the water flux is given by an extension of Darcy's law to unsaturated conditions [*Buckingham*, 1907; *Richards*, 1931; *Muskat and Meres*, 1936; *Muskat et al.*, 1937; see also *Bear*, 1972].

[19] Richards' equation is unable to reproduce the fingering phenomenon. This was explicitly conjectured, supported by numerical simulations, by *Eliassi and Glass* [2001], who employed typical constitutive relations for k_r and ψ, and hysteretic effects. The stability of Richards' equation has been much debated using theoretical and numerical analysis [*Diment et al.*, 1982; *Diment and Watson*, 1983; *Kapoor*, 1996; *Ursino*, 2000; *Du et al.*, 2001; *Egorov et al.*, 2003], until recent papers [*van Duijn et al.*, 2004; *Nieber et al.*, 2005; *Fürst et al.*, 2009] prove that Richards' equation is totally stable, to infinitesimal and finite-size perturbations, with or without hysteresis, and in a modal (asymptotic) and nonmodal (transient) sense. The appellative "totally stable" is, in this context, a very negative one: the analogue in fluid mechanics would be that the Navier-Stokes equations of fluid motion did not have the ability to produce turbulent solutions. The relevant pattern-forming physical mechanisms are therefore missing in the classical model of unsaturated flow in porous media.

[20] Many researchers have proposed extended theories of multiphase flow that depart from the traditional Darcy-like formulation. Here, we review some of them, restricting our attention to those directly related to extended models of unsaturated flow.

[21] On the basis of volume averaging of the microscopic equations of conservation of mass and momentum, Hassanizadeh and Gray identified that additional terms should be present in the macroscopic equations [*Hassanizadeh and Gray*, 1990, 1993a, 1993b]. In particular, they introduced the concept of dynamic capillary pressure, which has been the subject of intense experimental [*Hassanizadeh et al.*, 2002; *O'Carroll et al.*, 2005], modeling [*Beliaev and Hassanizadeh*, 2001; *Dahle et al.*, 2005; *DiCarlo*, 2005; *Manthey et al.*, 2005; *Mirzaei and Das*, 2006; *Helmig et al.*, 2007], and theoretical research [*Cuesta et al.*, 2000; *Cuesta and Hulshof*, 2003; *Egorov et al.*, 2003; *Nieber et al.*, 2005]. The concept of a "dynamic", rate-dependent, macroscopic capillary pressure has also been postulated independently by other authors [see, e.g., *Stauffer*, 1978; *Weitz et al.*, 1987; *del Rio and de Haro*, 1991]. The dynamic capillary pressure extension leads to a mixed third-order term (second order in space, first order in time), also known as relaxation term.

[22] *Cuesta et al.* [2000] analyzed a mathematical model of infiltration with a relaxation term, establishing existence of traveling wave solutions which exhibit oscillatory (nonmonotonic) behavior if the effect of dynamic capillary pressure is sufficiently large. *DiCarlo* [2005] reached similar conclusions; he used the relaxation term to achieve an analytic nonmonotonic solution by using the traveling wave properties of the observed infiltrations. The solutions were only nonmonotonic when the applied flux is above a critical flux, which depended on the magnitude of the additional term and the media properties. *Nieber et al.* [2005] gave a review of mathematical analyses of Richards' equation with static and dynamic capillary pressure-saturation relationships. In addition to a thorough stability analysis of the equations, nonmonotonic analytical solutions were found when a relaxation term (due to dynamic capillary pressure) was included.

[23] *Eliassi and Glass* [2002] introduced the hold-back–pileup effect, and conjectured it is the mechanism responsible for gravity fingering. They proposed three different extensions of the traditional Richards' equation: a hypodiffusive model (second order in space), a hyperbolic model (second order in time), and a mixed model (second order in space and first order in time). The hypodiffusive model is equivalent to the use of a nonmonotonic capillary pressure curve [*Eliassi and Glass*, 2003; *DiCarlo et al.*, 2008]. The hyperbolic model is analogous to the Cattaneo extension of

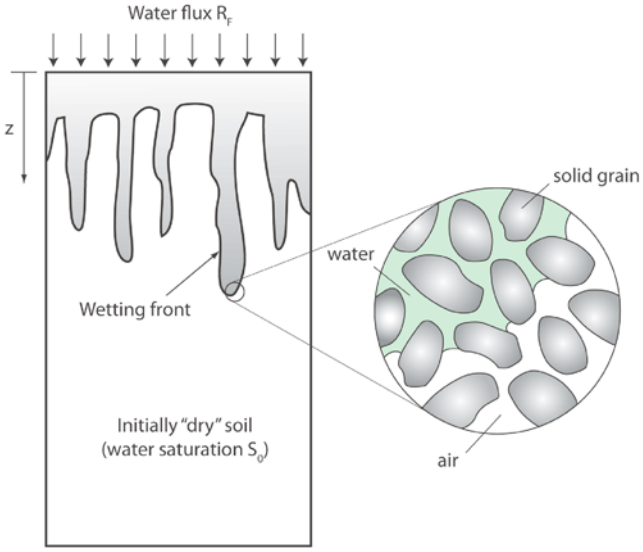

Figure 1. Schematic of vertical infiltration of water into a porous medium. Initially, the soil is almost dry (water saturation S_0). A constant and uniformly distributed flux of water R_F (LT^{-1}) is allowed to infiltrate into the soil. The flux of water is less than the hydraulic conductivity of the soil, K_s, so that the flux ratio is $R_s = R_F/K_s < 1$. Macroscopically, a diffuse interface (the wetting front) moves downward. This interface is often unstable and takes the form of long and narrow fingers that travel faster than the base of the wetting front [see, e.g., *Glass et al.*, 1989b, Figure 2]. Microscopically, a sharp interface between water and air exists (see inset), which is locally governed by capillary effects. From *Cueto-Felgueroso and Juanes* [2008]. Copyright 2008 by the American Physical Society.

the heat equation [*Cattaneo*, 1958; *Compte and Metzler*, 1997]. The mixed term can be related to the dynamic capillary pressure concept of *Hassanizadeh and Gray* [1993a]. Their numerical simulations [*Eliassi and Glass*, 2003] showed nonmonotonic behavior in the saturation profile, if the magnitude of the added terms is sufficiently large. The hypodiffusive and hyperbolic terms are antidiffusive and the resulting mathematical models, in the range of nonmonotonic solutions, are not well posed (they behave asymptotically as a backward heat equation). The hypodiffusive and hyperbolic extensions of Richards' equation proposed by *Eliassi and Glass* [2002, 2003] were analyzed by *DiCarlo et al.* [2008], who obtained traveling wave solutions that display, indeed, saturation overshoot. The models require, however, a regularization term to be well posed (analytical solutions were found with a third-order regularization term). Other works have included hysteresis effects in the capillary pressure, in addition to the dynamic (nonequilibrium) effects [*Nieber et al.*, 2003; *Sander et al.*, 2008].

[24] Nevertheless, all of these extensions do not address two important issues. First, they do not provide good quantitative agreement with experiments of saturation overshoot [*DiCarlo*, 2004]; in most cases the saturation is not bounded between 0 and 1 [*Cuesta et al.*, 2000; *Eliassi and Glass*, 2003; *DiCarlo*, 2005]. Second, they do not predict the finger width and finger velocity measured experimentally [*Glass et al.*, 1989b; *Selker et al.*, 1992b].

[25] A model related to the one proposed here was mentioned in passing by *DiCarlo et al.* [2008, p. 5] with reference to *Witelski* [1996], in which a fourth-order term is introduced in the formulation. This term, however, appears simply as a regularization term of strength $\varepsilon \to 0$, which allows for the recovery of well posedness of the equation when a nonmonotonic capillary pressure is used. Here, we introduce a fourth-order spatial derivative of finite magnitude, responsible for the dynamics of the wetting front (Figure 1).

3. Flow of Thin Films

[26] An everyday example of fingered flow is that of fluid down a slope (such as water on a windshield). In fact, the nature and appearance of this instability is remarkably similar to the one observed during infiltration in dry homogeneous sands (Figure 2).

[27] A mathematical model that explains the instability of the flow of thin films was first presented by *Huppert* [1982]. The important observation was that the dynamics of the thin film required a fourth-order derivative in space, a term associated with surface tension, to explain the instability. The model of thin films has been subsequently analyzed thoroughly [see, e.g., *Bertozzi and Brenner*, 1997], confirming the critical role of the fourth-order term.

[28] Consider the flow of a fluid film down a plane (Figure 3). The equation governing the film thickness, h [L], is [*Huppert*, 1982]:

$$\frac{\partial h}{\partial t} + \nabla \cdot \left[\frac{\rho g h^3}{3\mu} \left(\sin\alpha \nabla z - \cos\alpha \nabla h + \frac{\gamma}{\rho g} \nabla(\nabla^2 h) \right) \right] = 0, \quad (2)$$

where ρ [ML^{-3}] is the density of the fluid, μ [$ML^{-1}T^{-1}$] is the fluid dynamic viscosity, g [LT^{-2}] is the gravitational acceleration, α [$-$] is the angle of the plane with the horizontal, z [L] is the coordinate down the gradient of the inclined plane, and γ [MT^{-2}] is the surface tension.

[29] Comparing the thin-film equation (2) with Richards' equation (1), we can establish a one-to-one correspondence between the accumulation term, the viscous resistance, the advection term due to gravity, and the nonlinear diffusion term because of viscosity in the thin-film equation and because of microscopic capillarity in Richards' equation. The thin-film equation, however, contains an additional fourth-order term that models the effect of surface tension, which is missing in Richards' equation.

[30] Given the similarity in the flow patterns of both phenomena (Figure 2), it is tempting to add a fourth-order term to Richards' equation, and understand the new term as a macroscopic surface tension that operates at the finger scale (centimeters to decimeters) rather than the pore scale [*Chuoke et al.*, 1959; *Weitz et al.*, 1987; *DiCarlo and Blunt*, 2000]. This is indeed what we will do, and the model will be cast in the general framework of phase field models, which will endow the formulation with a rigorous thermodynamic foundation.

4. Phase Field Models of Interface Dynamics

[31] Phase field models have their origin in the mathematical description of phase transitions and solidification processes [*Cahn and Hilliard*, 1958; *Cahn*, 1961]. They are

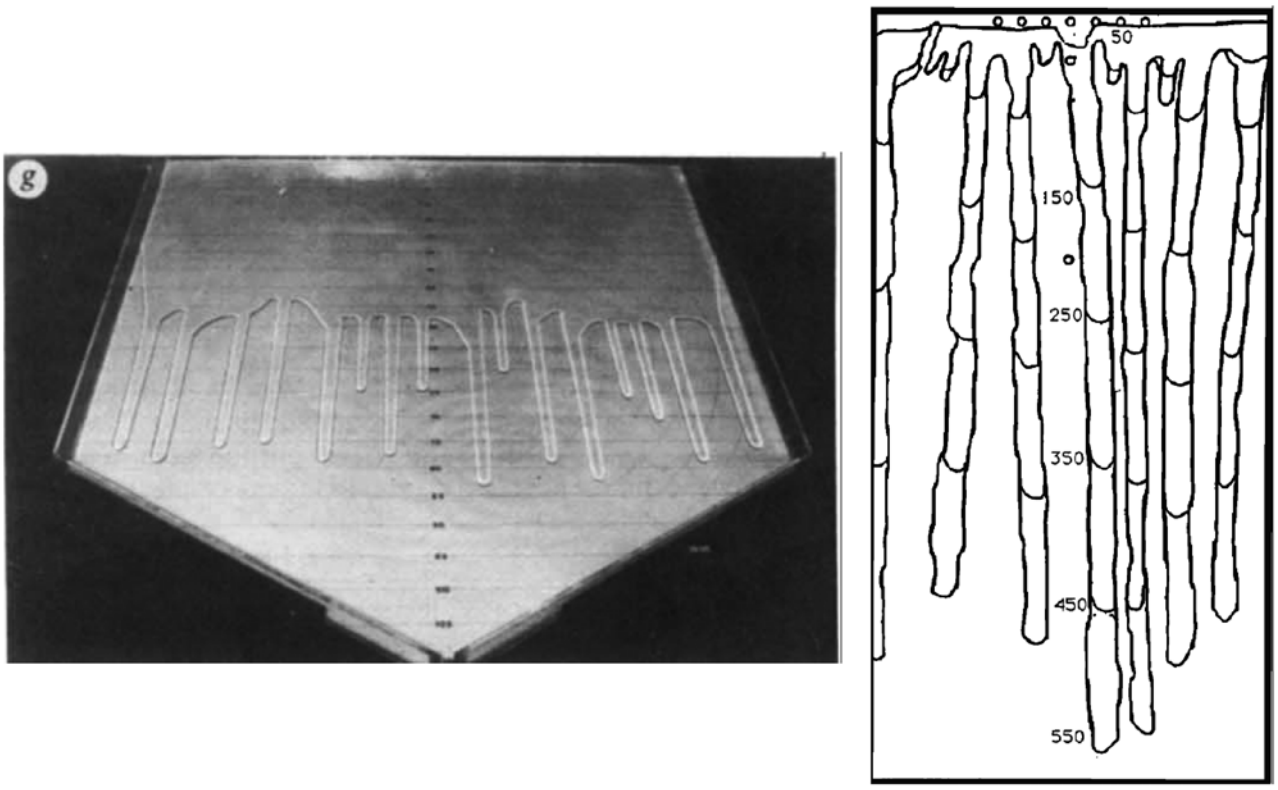

Figure 2. (left) The instability observed in the flow of a thin film of fluid down a plane [from *Huppert*, 1982] (reprinted by permission from Macmillan Publishers Ltd: Nature, copyright 1982) is remarkably similar to (right) that during infiltration in a dry homogeneous sand [from *Selker et al.*, 1992b]. Therefore we use the well-known equations governing thin-film flow as the basis for our model of unsaturated flow in porous media.

based on two key ideas: (1) the idea of expressing the energy of the system accounting for the fact that the system is not homogeneous and that macroscopic interfaces exist and (2) the idea that a sharp macroscopic interface is replaced by a diffuse interface (Figure 4). This is done by introducing an ''order parameter'' φ (the phase field) that ''labels'' the two macroscopic bulk phases (say, liquid and gas) and, in the sharp interface limit, recovers the interface evolution equations [*Elder et al.*, 2001].

[32] Naturally, the energy functional includes nonlocal terms that involve the gradient (and possibly higher-order derivatives) of the order parameter φ. In the simplest case, and because certain terms are ruled out because of symme-

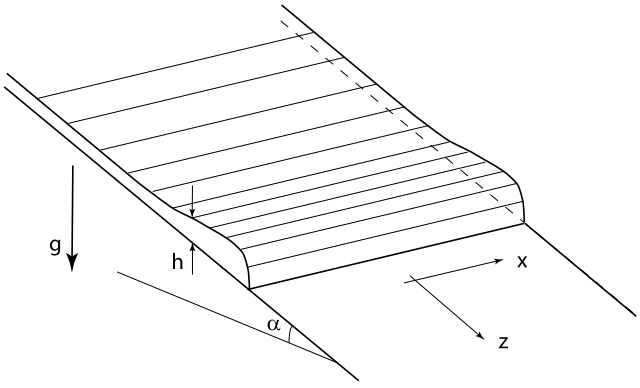

Figure 3. Sketch of the flow of a thin film of fluid down a plane at a slope (angle α with the horizontal). The thickness of the fluid film, h, is typically nonmonotonic, showing a hump near the wetting front and then decaying to an asymptotic value.

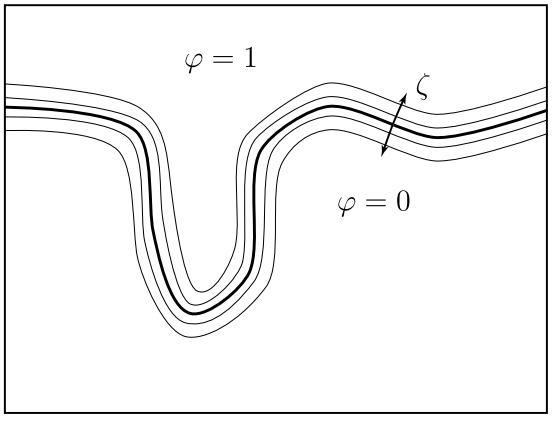

Figure 4. Schematic diagram of the key elements of a phase field model. The model introduces an order parameter φ that labels the bulk phases. A macroscopic interface (thick solid line) is replaced by a diffuse interface of thickness ζ, which corresponds to a region of high gradients of φ.

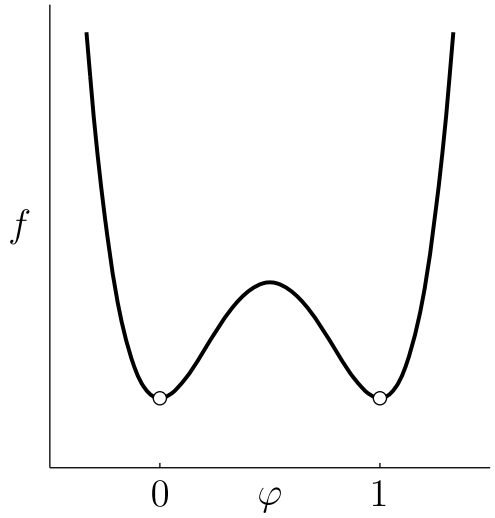

Figure 5. Typical bulk energy double-well potential in phase field models of binary transitions and solidification. The function is locally convex around two local minima, $\varphi = 0, 1$, which correspond to thermodynamically stable states. In general, for asymmetric potentials the stable states are determined through the classical convex hull construction [*Bray*, 1994].

try considerations, the free energy per unit volume of the system takes the form [*Bray*, 1994]:

$$\mathcal{E} = \mathcal{E}_{\text{bulk}} + \mathcal{E}_{\text{interf}} = f(\varphi) + \frac{\varepsilon}{2}|\nabla\varphi|^2. \quad (3)$$

[33] In phase separation problems, the function f is typically a double-well potential (Figure 5), in which the local minima correspond to the homogeneous stable states [*Cahn and Hilliard*, 1958; *Bray*, 1994]. The gradient square term makes the evolution of the inhomogeneous system well posed. As we will see in section 5.4, however, the bulk energy function in our model of unsaturated flow is very different from a double-well potential.

[34] The chemical potential of the system is the variational derivative of the free energy functional. The phase field equations of the model can then be obtained by invoking mass conservation and a gradient-type flux [*Bray*, 1994; *Emmerich*, 2008]. In section 5, we will illustrate this formalism with the development of a phase field model of unsaturated flow.

[35] This type of models has been used to describe a variety of physical and biological phenomena, such as epitaxial growth of surfaces [*Langer*, 1989; *Karma and Rappel*, 1996; *Gollub and Langer*, 1999], binary transitions [*Lowengrub and Truskinovsky*, 1998], and solidification [*Cahn and Hilliard*, 1958; *Cahn*, 1961; *Boettinger et al.*, 2002; *Emmerich*, 2008].

[36] The statistical physics community has employed this type of formulation to describe imbibition into random media [*Dubé et al.*, 1999, 2000a, 2000b, 2001; *Alava et al.*, 2004; *Dubé et al.*, 2007] and Hele-Shaw cells with disorder [*Hernández-Machado et al.*, 2001; *Soriano et al.*, 2002, 2005]. These models have been used to understand the roughening of stable imbibition fronts, generalizing the description of interface dynamics put forward by Kardar-Parisi-Zhang [*Kardar et al.*, 1986] (see also *Horvath et al.* [1991], *Buldyrev et al.* [1992], *He et al.* [1992], *Horvath and Stanley* [1995], and *Lopez* [1999] and the review by *Halpin-Healy and Zhang* [1995]), in order to satisfy mass conservation [*Sun et al.*, 1989; *Kim and Das Sarma*, 1994].

[37] In these models, however, a double-well potential is assumed and, as a result, the flow physics in the bulk is overly simplified. The models only capture a "wet" and a "dry" region, without smooth changes in saturation in the wet region. The models have been designed for the analysis of stable fronts only (such as upward imbibition with stabilizing gravity, with or without the stabilizing effect of evaporation), and cannot model unstable infiltration or predict the onset of fingering.

[38] A related model was proposed by Papatzacos [*Papatzacos*, 2002; *Papatzacos and Skjæveland*, 2004, 2006] where, assuming a diffuse interface model at the pore level, a Cahn-Hilliard equation is obtained to describe macroscopic two-phase flow. The model is developed for a single-component system with phase change, and the proposed energy potential is also of double-well type.

5. A Phase Field Model of Unsaturated Flow

5.1. Analogy With Thin Films

[39] Driven by the analogy with the thin-film equation (2), we propose to add to Richards' equation (1) a fourth-order term that is responsible for a macroscopic surface tension effect:

$$\phi\frac{\partial S}{\partial t} + \nabla\cdot\left[K_s k_r(S)\left(\nabla z + \nabla\psi(S) + \frac{\Gamma}{\rho g}\nabla(\nabla^2 S)\right)\right] = 0, \quad (4)$$

where Γ [MT^{-2}] plays the role of such macroscopic surface tension. The model was first proposed by *Cueto-Felgueroso and Juanes* [2008], and its stability characteristics were subsequently analyzed by *Cueto-Felgueroso and Juanes* [2009b]. Far away from the region of high-saturation gradients (the wetting front), the equation reduces to Richards' equation. Near the interface, however, the fourth-order term becomes dominant. The model is analogous to the equation describing the flow of thin films except that the scaling of the various terms is different.

[40] As we will see in section 6, the model is able to reproduce a nonmonotonic saturation profile, believed to be an essential feature of fingered flows. In the 2-D simulations, we will show that this is indeed the case, and that the fourth-order term allows us to explain the formation of fingers during infiltration.

5.2. Phase Field Framework

[41] The proposed governing equation for infiltration can be derived from the powerful framework of phase field models, without any analogy to thin-film flows. Water mass conservation leads to an evolution equation for the water saturation S:

$$\frac{\partial(\rho\phi S)}{\partial t} + \nabla\cdot\mathbf{J} = 0, \quad (5)$$

where $\mathbf{J}$ [$\mathrm{ML^{-2}T^{-1}}$] is the water mass flux. We adopt a gradient flow formulation [see, e.g., *Emmerich*, 2008],

$$\mathbf{J} = -\rho\lambda\nabla\Phi, \tag{6}$$

where λ [$\mathrm{M^{-1}L^3T}$] is the water mobility, and Φ [$\mathrm{ML^{-1}T^{-2}}$] is the flow potential. The water mobility includes the effect of reduced permeability to water due to partial saturation, and takes the form:

$$\lambda = \frac{k}{\mu}k_r(S). \tag{7}$$

[42] Under unsaturated conditions (water saturation strictly less than one), it is well justified to make two assumptions [*Bear*, 1972; *Philip*, 1969]. First, air is infinitely mobile compared to water and, as a result, the air pressure remains constant and equal to atmospheric pressure. The water pressure is then equal to the negative suction (or capillary pressure):

$$p_{\mathrm{water}} = \underbrace{p_{\mathrm{air}}}_{=0} - P_c(S). \tag{8}$$

The capillary pressure is a monotonically decreasing but often nonconvex function of water saturation [*Bear*, 1972]. The second assumption is that the compressibility of water and rock is negligible compared to that of air, and therefore the water density ρ and the porosity ϕ are constant.

[43] Under these conditions, we write the free energy per unit volume of the system as:

$$\mathcal{E} = \mathcal{E}_{\mathrm{gr}} + \mathcal{E}_{\mathrm{cap}} + \mathcal{E}_{\mathrm{nl}} = \underbrace{-\rho g S z + \Psi(S)}_{\mathrm{local}} + \underbrace{\frac{1}{2}\Gamma|\nabla S|^2}_{\mathrm{nonlocal}}, \tag{9}$$

which comprises the gravitational ($\mathcal{E}_{\mathrm{gr}}$) and capillary pressure ($\mathcal{E}_{\mathrm{cap}}$) energy potentials, as well as a nonlocal energy potential ($\mathcal{E}_{\mathrm{nl}}$). The capillary pressure function is derived from the capillary potential:

$$P_c(S) = -\frac{d\Psi}{dS}, \tag{10}$$

which we can further express in head units [L]:

$$\psi(S) = \frac{1}{\rho g}P_c(S). \tag{11}$$

The nonlocal term models the extra energetic cost associated with the displacement of water-air interfaces in areas of large saturation gradients. The coefficient Γ plays the role of an apparent surface tension associated with the wetting front [*Huppert*, 1982; *Weitz et al.*, 1987; *DiCarlo and Blunt*, 2000].

[44] The flow potential Φ is the variational derivative of the free energy:

$$\Phi = \frac{\delta\mathcal{E}}{\delta S} = \frac{\partial\mathcal{E}}{\partial S} - \nabla\cdot\left(\frac{\partial\mathcal{E}}{\partial\nabla S}\right) = -\rho g z - \rho g\psi(S) - \Gamma\nabla^2 S. \tag{12}$$

Combining equations (5), (6), and (12), and the unsaturated flow assumptions of constant water density and porosity, we arrive at the proposed model equation (4):

$$\phi\frac{\partial S}{\partial t} + \nabla\cdot\left[\frac{k\rho g}{\mu}k_r(S)\left(\nabla z + \nabla\psi(S) + \frac{\Gamma}{\rho g}\nabla(\nabla^2 S)\right)\right] = 0, \tag{13}$$

where we identify the saturated hydraulic conductivity, $K_s = k\rho g/\mu$. The traditional Richards equation (1) can be recovered by neglecting the nonlocal energy term in equation (13).

5.3. Scaling of the Fourth-Order Term

[45] The question arises: what is the value of the coefficient Γ that scales the fourth-order term? To address this question, we consider the vertical volumetric flux at a point in the transition region of the wetting front, of thickness ζ (Figure 4):

$$q_v = K_s k_r(S)\left(1 + \frac{\partial\psi}{\partial z} + \Lambda\frac{\partial\nabla^2 S}{\partial z}\right), \tag{14}$$

where $\Lambda = \Gamma/(\rho g)$. The suction head is expressed as:

$$\psi(S) = h_{\mathrm{cap}}J(S), \tag{15}$$

where $J(S)$ [$-$] is a dimensionless capillary pressure function, and h_{cap} [L] is the capillary rise, whose dependence on the system parameters is given by the classical Leverett scaling [*Leverett*, 1941]:

$$h_{\mathrm{cap}} \sim \frac{\gamma\cos\theta}{\rho g\sqrt{k/\phi}}, \tag{16}$$

where γ is the surface tension between the fluids, and θ [$-$] is an effective contact angle. It is well known [see, e.g., *Selker and Schroth*, 1998] that this effective contact angle is, in general, different from the microscopic contact angle between the air-water interface and the solid surface [*de Gennes*, 1985]. Indeed, pore-scale modeling studies show that a relatively wide range of contact angles must be used to reproduce imbibition capillary pressure and relative permeability curves, even in water-wet media [*Valvatne and Blunt*, 2004]. In any case, the relevant quantity, and the only one that is used in our theory, is the capillary height h_{cap} (which incorporates the surface tension of the pair of fluids, the characteristic microscopic length scale of the medium, and the wetting characteristics).

[46] The parameter Λ has dimensions of $\mathrm{L^3}$. One possibility is to understand it as a (new) free parameter. We find this choice unattractive, for several reasons. First, one can argue that by introducing a new parameter, it is "easy" to reproduce experimental data. Second, one should then provide a methodology to determine the new parameter experimentally. And third, it is unclear what would be the new physical property (not present in Richards' equation) that gives rise to an independent parameter in the system. We argue, instead, that the system can be described with the physical properties already present: gravity, viscous resistance, and microscopic surface tension.

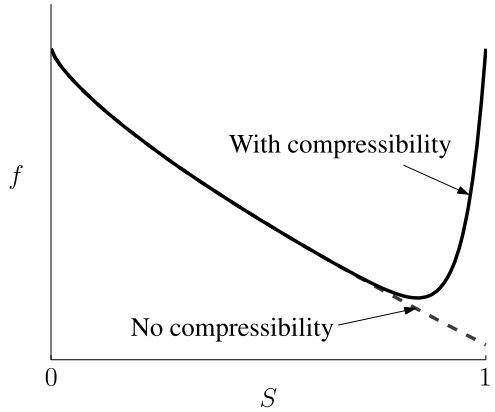

Figure 6. The dashed line is a typical capillary energy potential in our phase field model of unsaturated flow. The function is monotonically decreasing, and values of water saturation above one are favored. The solid line is the combined energy potential when a compressibility term is added to the formulation. The new function has a minimum near $S = 1$, which serves as an attractor for the phase field variable. Saturation values above one are disallowed.

[47] We analyze the scaling of the capillary and nonlocal terms at the wetting front. The capillary term scales like h_{cap}/ζ. Therefore gravity and capillarity are both important at the wetting front if $\zeta \sim h_{\text{cap}}$, and their relative strength can be measured by the nondimensional group $Gr_\zeta = \zeta/h_{\text{cap}}$. The nonlocal term resembles a curvature-driven flux, where the Laplacian can be expressed as [*Weatherburn*, 1927; *Lei*, 1988]:

$$\nabla^2 S = \frac{\partial^2 S}{\partial n^2} + \kappa_H |\nabla S|, \tag{17}$$

where n is the space coordinate perpendicular to the front, and κ_H is the in-plane curvature of the front. Therefore we have the scaling:

$$\Lambda \frac{\partial \nabla^2 S}{\partial z} \sim \Lambda \frac{1}{\zeta^3}. \tag{18}$$

To have an $O(1)$ term, we must have $\Lambda \sim \zeta^3$ and, from the scaling of the capillary term, $\Lambda \sim h_{\text{cap}}^3$. The relative strength of gravity to macroscopic surface tension effects is measured by the nondimensional group:

$$N\ell_\zeta = \frac{\Lambda}{\zeta^3} \sim \frac{h_{\text{cap}}^3}{\zeta^3} = Gr_\zeta^{-3}. \tag{19}$$

This scaling is not coincidental: it is required to retain the balance among the different terms in the sharp interface limit $\zeta \to 0$ [*Elder et al.*, 2001]. If one chooses $N\ell_\zeta = Gr_\zeta^{-\alpha}$ with $\alpha < 3$, the sharp interface limit corresponds to Richards' equation. If $\alpha > 3$, imbibition is governed in the sharp interface limit purely by curvature-driven flow, an unphysical model.

[48] In general, the coefficient of proportionality relating $N\ell_\zeta$ and Gr_ζ^{-3} will depend on the rest of the properties of the system, such as initial saturation S_0, flux ratio R_s, and relative permeability and capillary pressure characteristics. For simplicity, here we take

$$N\ell_\zeta = Gr_\zeta^{-3}. \tag{20}$$

[49] As a summary, we express the mathematical model (13) in dimensionless form, by rescaling $\mathbf{x} \to \mathbf{x}/L$, where L is an arbitrary length, and $t \to t/T$, where $T = L\phi/K_s$. We define the following two nondimensional groups:

$$Gr = \frac{L}{h_{\text{cap}}} \quad \text{(gravity number)}, \tag{21}$$

$$N\ell = \frac{\Lambda}{L^3} \quad \text{(nonlocal number)}. \tag{22}$$

With the proposed scaling of equation (20), and understanding the space and time coordinates ($\mathbf{x}$, t) as their dimensionless counterparts, the model reads:

$$\frac{\partial S}{\partial t} + \nabla \cdot \left[k_r(S) \left(\nabla z + Gr^{-1} \nabla J(S) + Gr^{-3} \nabla \left(\nabla^2 S \right) \right) \right] = 0. \tag{23}$$

5.4. Refinement of the Model: Bounded Saturation Overshoot

[50] In the model as presented, the saturation overshoot is not bounded. That is, the solution to equation (13) may take values larger than one, clearly an unphysical situation. This is the case for most continuum extensions of Richards' equation [*Cuesta et al.*, 2000; *Cuesta and Hulshof*, 2003; *Eliassi and Glass*, 2002, 2003; *DiCarlo*, 2005]. *Nieber et al.* [2005] avoid overshoots above 1 in their dynamic relaxation model by the use of a relaxation term of the form $\tau \sim dP_c/dS$ and a van Genuchten capillary pressure function $P_c(S)$; overshoots above 1 appear if a Brooks-Corey capillary pressure function is used. *DiCarlo et al.* [2008] also guarantee saturations below 1, but in their case the high-order term is a regularization term of infinitesimal strength.

[51] The thermodynamic framework of phase field models indicates why saturations above 1 occur, and permits rectifying the model to yield a water saturation that is bounded between 0 and 1. When the medium approaches full saturation ($S \approx 1$), the two assumptions of infinite mobility and infinity compressibility of air cease to be valid. Just behind the wetting front, the water pressure is no longer the negative capillary suction [*Bauters et al.*, 1998]. Therefore the energy of the system must include an extra term because of the water pressure. From the point of view of phase field models, the saturation overshoot occurs because the bulk energy potential in equation (9), unlike the double-well potential, does not an have a preferred "stable" state. The capillary potential is given by

$$f_{\text{cap}}(S) = \int_S^1 \psi(s)\, ds. \tag{24}$$

Typically, this potential function is monotonically decreasing (Figure 6). Therefore the equations do not prevent the saturation from achieving unboundedly large values.

[52] Consider now an additional "compressibility" term in the bulk energy potential that introduces a boundary layer, such that the combined capillary-compressibility potential has a minimum near $S = 1$ (Figure 6). This minimum acts as an attractor for the phase-ordering parameter, and values of water saturation above one do not occur. We will see the effect clearly in the simulations of section 6.

6. Simulation Results

[53] The mathematical model is given by equation (23), together with appropriate initial and boundary conditions, and constitutive relations. It is assumed that the initial water saturation S_0 is uniform, and that the infiltration rate R_F [LT^{-1}] is uniformly distributed and constant in time (see Figure 1). The infiltration rate R_F may be expressed as a flux ratio, $R_s = R_F/K_s$, with $R_s \in [0, 1]$.

[54] We adopt a power law relative permeability of the form

$$k_v(S) = S^b, \tag{25}$$

and a Brooks-Corey capillary pressure function [*Brooks and Corey*, 1966],

$$J(S) = S^{-1/\lambda}, \tag{26}$$

which yields a capillary potential

$$f_{\text{cap}}(S) = -\frac{\lambda}{\lambda - 1} S^{1-1/\lambda}. \tag{27}$$

We adopt an exponential compressibility potential of the form

$$f_{\text{comp}}(S) = \exp(-\kappa(1 - S)) f_{\text{cap}}(S). \tag{28}$$

Hence, the total bulk free energy is given by

$$f(S) = f_{\text{cap}}(S) + f_{\text{comp}}(S) = -\frac{\lambda}{\lambda - 1} S^{1-1/\lambda}[1 - \exp(-\kappa(1 - S))]. \tag{29}$$

6.1. Traveling Waves

[55] We present traveling wave solutions to equation (23), which represent 1-D infiltration fronts. Although we addressed their practical computation elsewhere [*Cueto-Felgueroso and Juanes*, 2009a], we include some examples here in order to set the framework for the analysis of the saturation overshoot and wetting front stability.

[56] The traveling wave solutions are computed using an adaptive rational spectral method with adaptively transformed Chebyshev nodes, which does not require that the underlying problem is transformed into new coordinates [*Tee and Trefethen*, 2006; *Cueto-Felgueroso and Juanes*, 2009a]. The method takes into account, and locates, a priori unknown singularities of the underlying solution. We use conformal mapping to design transformed nodes that improve the Chebyshev spectral method. Chebyshev-Padé approximation is used to determine the locations of the singularities of the solution in the complex plane. This type of discretization has allowed us to compute accurate traveling waves and eigenvalues for very small values of the initial water saturation, using just a few hundred grid points.

[57] Traveling wave solutions to our model display a nonmonotonic saturation profile, with a sharp wetting front, a saturation overshoot at the tip, and a decay to an asymptotic saturation value S_- (Figure 7). Changes in the gravity number Gr induce changes in the scale of the solution, and thus the length scale of the bump increases like Gr^{-1} (Figure 7a). Stronger capillary dissipation, given in terms of the Brooks-Corey parameter λ, results in a stabilization of the wetting front, and a smaller saturation overshoot (Figure 7b). Even slight increases in the initial saturation S_0 have a strong influence on the saturation overshoot: the magnitude of the overshoot decreases as the initial saturation increases (Figure 7c). The flux ratio R_s also plays a critical role in the structure and stability of the front. The overshoot increases with the flux ratio, until the tip reaches saturations close to one (Figure 7d). The behavior near $S = 1$ is fundamentally influenced by the compressibility model, through the parameter κ.

[58] To elucidate the influence of the compressibility model, we compute traveling waves for the same flux ratio and water relative permeability function, but changing the compressibility parameter κ. As the minimum of the bulk free energy moves toward 1 (increasing κ), the maximum saturation attained also approaches 1 (Figure 8a). This maximum saturation depends not only on the position of the minimum in the bulk free energy, but also on the nonlinearity of the relative permeability curve. Highly nonlinear conductivities, corresponding to larger values of the exponent b, result in larger saturation overshoots (Figure 8b). Indeed, one of the important insights of the present study is the dominant role of the relative permeability on the behavior of the saturation overshoot and subsequent fingering instability.

6.2. Comparison With Quasi-1-D Experiments of Infiltration

[59] In this section we compare the model predictions of saturation overshoot with laboratory measurements from quasi-1-D experiments of infiltration into homogeneous sands [*DiCarlo*, 2004].

[60] We first fit the unsaturated water conductivity measured experimentally to a piecewise polynomial:

$$k_r(S) \approx \begin{cases} P_1(S) = S^a & \text{if } S < S_\times, \\ P_2(S) = S^b & \text{if } S > S_\times, . \end{cases} \tag{30}$$

where $S_\times$ is the crossover saturation. Such crossover in the power law behavior from low water saturation to high water saturation is observed experimentally [*DiCarlo*, 2004, 2007]. A smooth curve is obtained using a blending function, such that:

$$k_r(S) = P_1(S)g(S) + P_2(S)(1 - g(S)), \tag{31}$$

where

$$g(S) = \frac{1}{2}(1 - \tanh(c(S - S_\times))). \tag{32}$$

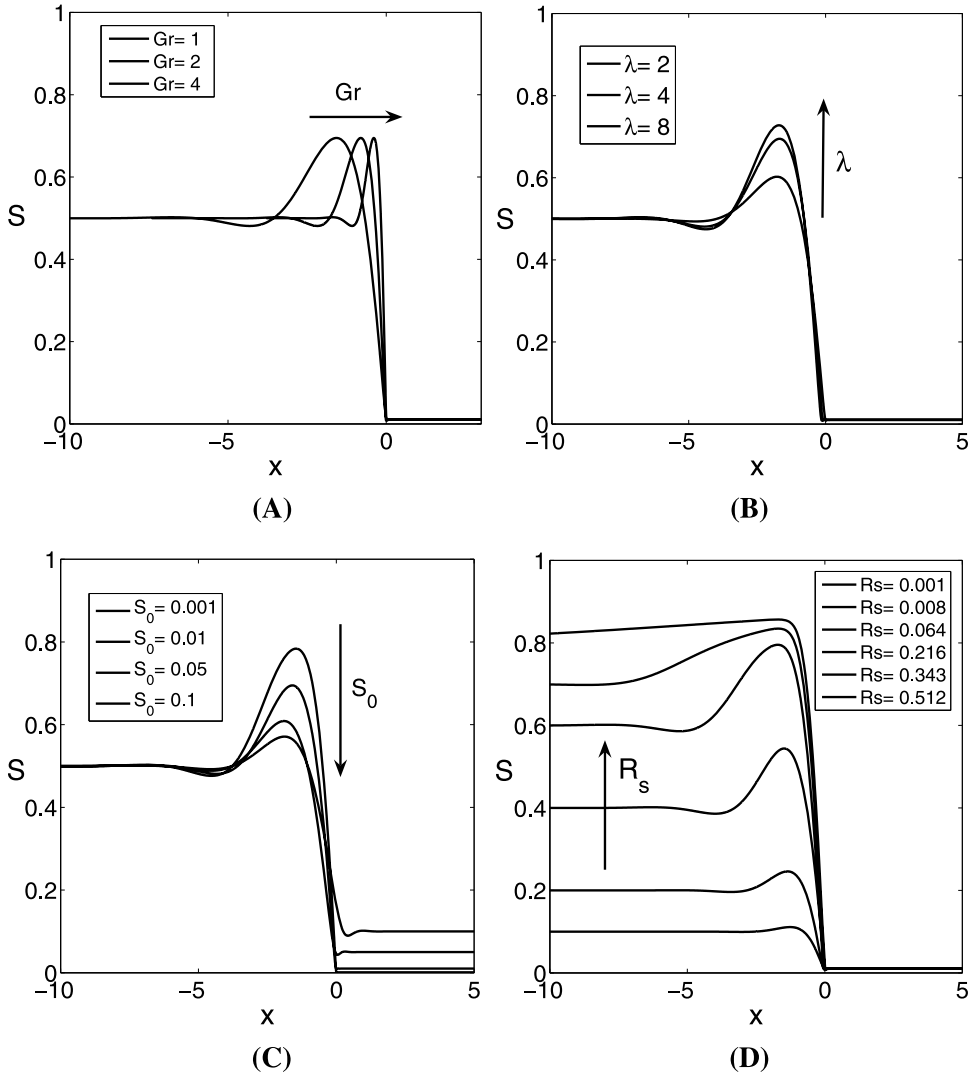

Figure 7. Influence of the model parameters on the traveling wave solutions to the proposed model. The default parameters are $k_r = S^3$, $\lambda = 4$, $\kappa = 20$, $S_- = 0.5$, and $S_0 = 0.01$. (a) Influence of the gravity number *Gr*. (b) Influence of the Brooks-Corey parameter λ. (c) Influence of the initial water saturation S_0. (d) Influence of the flux ratio $R_s = k_r(S_-)$.

The parameters a, b, c and $S_\times$ determined to fit the experimental curves of *DiCarlo* [2004] are given in Table 1, and the relative permeability functions are plotted in Figure 9.

[61] For the bulk free energies, we use generic Brooks-Corey capillary pressure functions, equation (26), with a parameter λ. The compressibility potentials (equation (28)), introduce the compressibility parameter κ. The values taken for DiCarlo's experiments are given in Table 1. The resulting bulk free energies and their derivatives with respect to saturation are plotted in Figure 10.

6.2.1. Saturation Overshoot

[62] We investigate the influence of the model parameters on the saturation overshoot by plotting the difference between the tip saturation S_{tip} and the tail saturation S_- against the flux ratio R_s (Figure 11). The most influential parameters are the initial saturation and the relative permeability function (Figures 11a and 11b, respectively). Large saturation overshoots are indicative of dry soils, with conductivities that behave like power laws with a large exponent, for which large water saturations are compatible with small fluxes. The form of the compressibility function has a mild influence in smoothing the overshoot for large flux ratios (Figure 11c), while the Brooks-Corey parameter λ has a relatively uniform effect over the whole range of flux ratios (Figure 11d).

[63] We compare the model predictions with the experimental measurements of *DiCarlo* [2004]. We have not intended to achieve a perfect fit of the experimental results by tuning the model parameters, but rather to show that the observed trends can be easily explained by the proposed theory. Nevertheless, we have fitted the experimental conductivity curves as closely as possible, as this appears to be the most critical constitutive relation, and the trends in saturation overshoot cannot be understood without capturing the highly nonlinear behavior of the measured conductivity curves. The initial saturation for all the dry sands is taken as $S_0 = 0.01$. This value was chosen by us; experi-

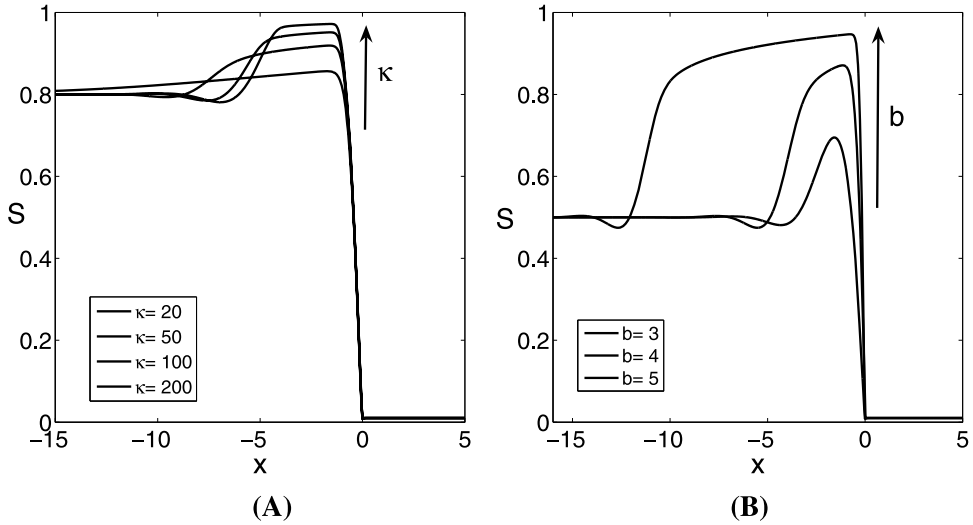

Figure 8. Influence of the compressibility term of the bulk free energy on the traveling wave solutions of the model. The default parameters are $k_r = S^3$, $\lambda = 4$, $\kappa = 20$, $S_- = 0.5$, and $S_0 = 0.01$. (a) Influence of the compressibility parameter κ. (b) Influence of the relative permeability function. We set $k_r = S^b$ and plot the traveling waves for different values of the exponent b.

mentally, the initial saturation was small enough that a numeric value was not reported by *DiCarlo* [2004].

[64] The 30/40 sand shows the "canonical" overshoot behavior, with compressibility effects restricted to the highest flux ratios (Figure 12a). For the coarser 20/30 sand, the transition to almost fully saturated tips is smoother, which is partially due to the structure of the conductivity curve, but also to the form of the bulk free energy (Figure 12b). We test the ability of our model to reproduce the saturation overshoot under different conditions, without changes in any of the parameters. Simulations using higher initial saturation show a reduced saturation overshoot, in agreement with experimental measurements (Figures 12c and 12d).

[65] *DiCarlo* [2004] presents as a paradox the fact that, while having similar capillary pressure–saturation properties, the 12/20 and grey sands exhibit radically different overshoot behavior. Our theory renders a simple explanation to their overshoot behavior: the relative permeability curves are very different. While this difference may be inconsequential within the classical theory, in our context this difference in essential. The 12/20 sand behaves as a very nonlinear power law until the medium reaches a certain saturation, whereas the grey sand behaves like a cubic function for most of the saturation range. This fact alone suffices to explain the observed differences (Figure 13).

[66] The accuracy of our predictions is notable, particularly taking into account that our only effort to reproduce the experimental conditions concerns the unsaturated conductivity curves. This fact also implies that the shape of the conductivity curve is critical in the behavior of the wetting front. It also implies that generic definitions usually employed in the literature, which give unsaturated conductivities that are quadratic or cubic, are not representative of sands that display large overshoots and wetting front instability.

6.2.2. Saturation Profiles

[67] According to classical interpretations of unsaturated flow, our model would have, at best, the ability to predict the saturation overshoot at the wetting front (as that involves primary imbibition alone) but should miss the shape of the saturation profile behind the wetting front [*Eliassi and Glass*, 2002; *DiCarlo*, 2007; *DiCarlo et al.*, 2008]. While it is true that the system undergoes drainage behind the front tip, and that the constitutive relations will in general be different from those in imbibition, our model predictions, without any hysteretic effects, are in good quantitative agreement with the saturation profiles measured experimentally (Figure 14). The far end of the profiles match the experimental curves because we fit the unsaturated conductivity. However, the transition behind the wetting front is also captured well with our model. We conclude that the characteristics and length scale of the saturation overshoot can be explained with a continuum model, using macroscopic concepts, and without introducing rate-dependent or history-dependent constitutive relations.

6.3. Two-Dimensional Simulations

[68] We present 2-D simulations of gravity fingering during constant-flux infiltration in heterogeneous soils. Results for homogeneous media were presented by *Cueto-Felgueroso and Juanes* [2008], where we showed the development of fingering instability, and analyzed the

Table 1. Parameters Chosen to Fit the Relative Permeability and Capillary Pressure Functions Measured Experimentally by *DiCarlo* [2004][a]

Sand	a	b	c	$S_\times$	λ	κ
30/40	11	2.0	10	0.35	4.0	20
20/30 (dry)	11	3.0	10	0.22	4.0	10
20/30 (wet)	11	2.7	10	0.22	4.0	10
12/20	11	2.7	20	0.22	1.5	10
Grey	11	3.0	20	0.12	1.5	10

[a]See text for the definition and explanation of each parameter.

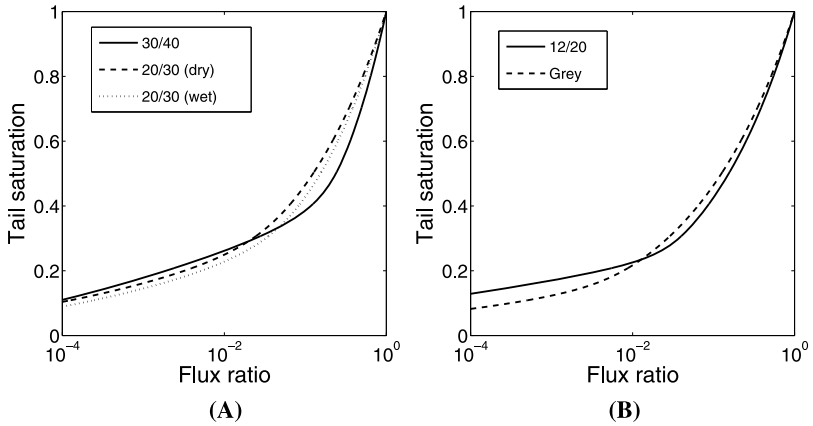

Figure 9. Relative permeability functions that fit the experimental results of *DiCarlo* [2004]: (a) 30/40 and 20/30 sands and (b) 12/20 and grey sands.

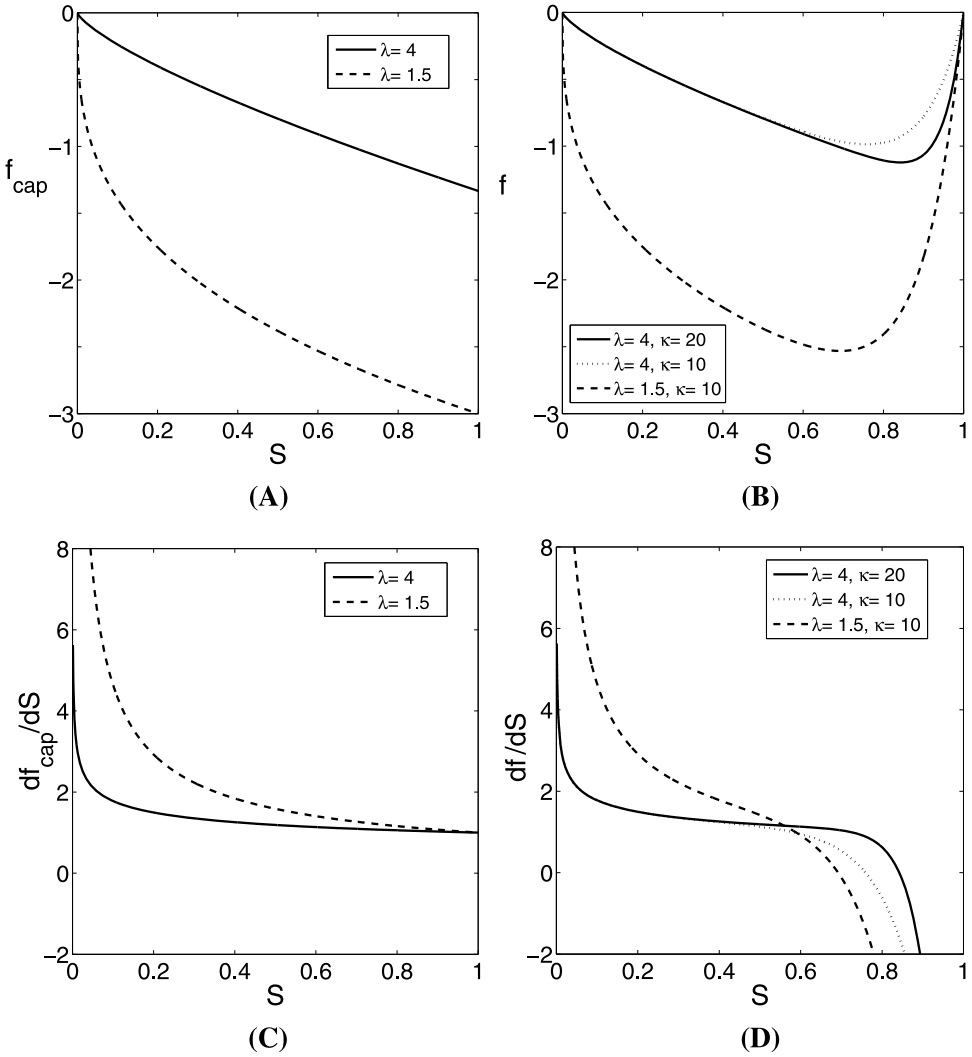

Figure 10. Bulk free energies f and their derivatives with respect to water saturation, $J = df/dS$. The (a) capillary free energies f_{cap} are constructed from (c) classical Brooks-Corey capillary pressure functions $J = df_{cap}/dS$. Adding the compressibility free energies, we obtain (b) the total bulk free energies $f = f_{cap} + f_{comp}$, whose derivative with respect to water saturation gives (d) the bulk flow potential, $\tilde{J} = df/dS$.

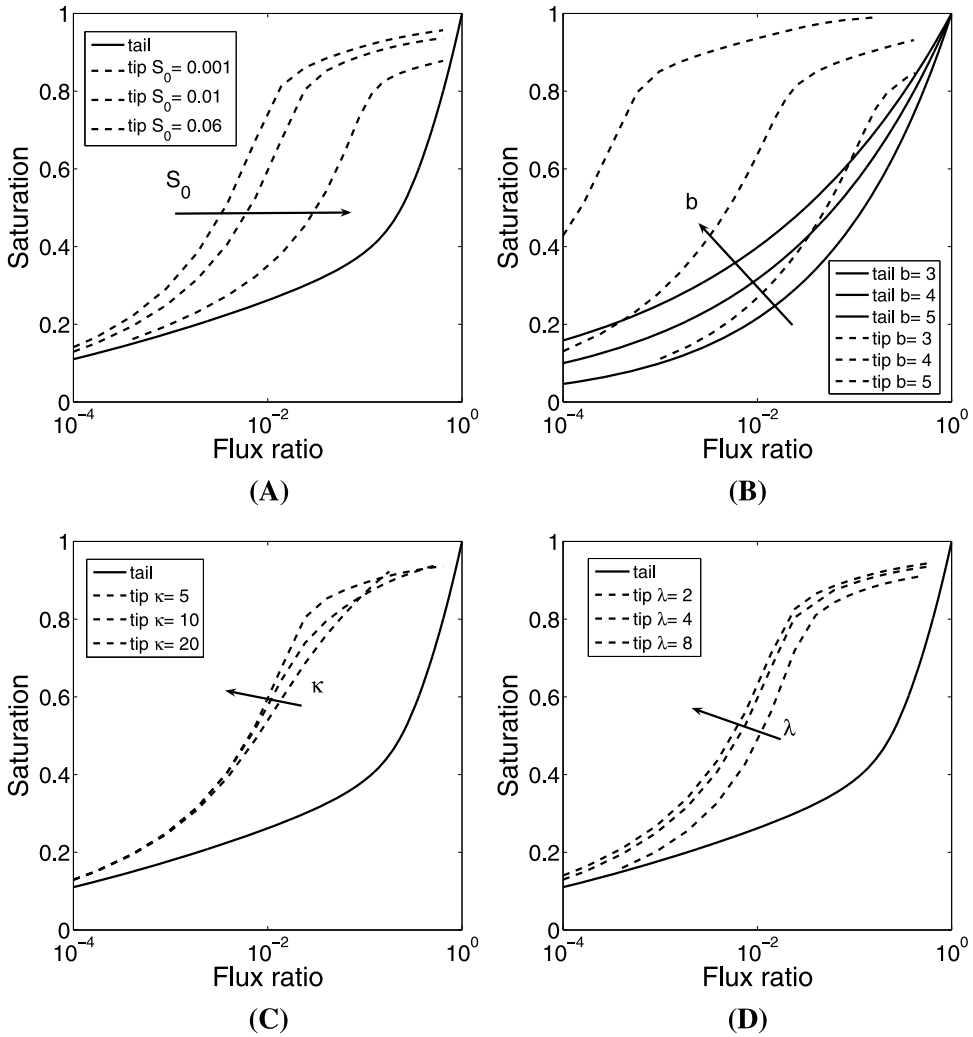

Figure 11. Influence of the model parameters on the saturation overshoot. The default properties are those of the 30/40 sand. (a) Initial saturation S_0. (b) Relative permeability power law exponent b. (c) Compressibility parameter κ. (d) Brooks-Corey parameter λ.

influence of the various system parameters on the fingered flow. The objective of the present simulations is to demonstrate the effect of mild heterogeneity in the finger evolution, and the critical role played by the nonlinearity of the relative permeability function. We consider heterogeneity in the absolute permeability, but assume that it does not affect the form of the relative permeability or capillary pressure functions.

[69] The computational domain is the rectangle $[-2, 2] \times [-1, 1]$, and the gravity number is set to $Gr = 20$. For the capillary pressure function we use a standard van Genuchten-Mualem model [*Mualem*, 1976; *van Genuchten*, 1980] with $n = 10$ and $m = 1 - 1/n$. The relative permeability is a simple polynomial function, $k_r = S^9$. We use two permeability fields. The first has a short correlation length, with range $r \approx 0.08$. The permeability follows a lognormal distribution with mild heterogeneity: $k_{\max}/k_{\min} \approx 25$, and $\sigma^2_{\ln k} \approx 0.16$ (Figure 15a). The second permeability field is generated by filtering the fine-scale one to obtain a finger-scale correlation length (range $r \approx 0.16$), while keeping the ratio $k_{\max}/k_{\min} \approx 25$ (Figure 15c).

[70] The domain is periodic in the horizontal direction. The initial saturation is $S_0 = 0.01$. The saturation at the top boundary is $S_- = 0.4$, corresponding to a flux ratio $R_s = 2.62 \times 10^{-4}$. The flow is initialized assuming a perturbed, flat front near the top of the domain.

[71] The numerical simulation of the proposed model in multiple dimensions is significantly more demanding than similar computations with Richards' equation. Moreover, the field of numerical methods for higher-order equations is still in its infancy. In the present context, the reference point is previous work on numerical simulation of the Cahn-Hilliard equation [see, e.g., *Cueto-Felgueroso and Peraire*, 2008; *Gomez et al.*, 2008], and thin-film flows [*Kondic*, 2003].

[72] Our simulations use eighth-order finite differences in the vertical direction, and Fourier expansions in the horizontal direction (which is assumed to be periodic). For the convective term, the stencil is slightly upwinded in order to avoid the spurious growth of unresolved high frequencies near the wetting front. The time integration is based on the semiimplicit method presented by *Zhu et al.* [1999], which

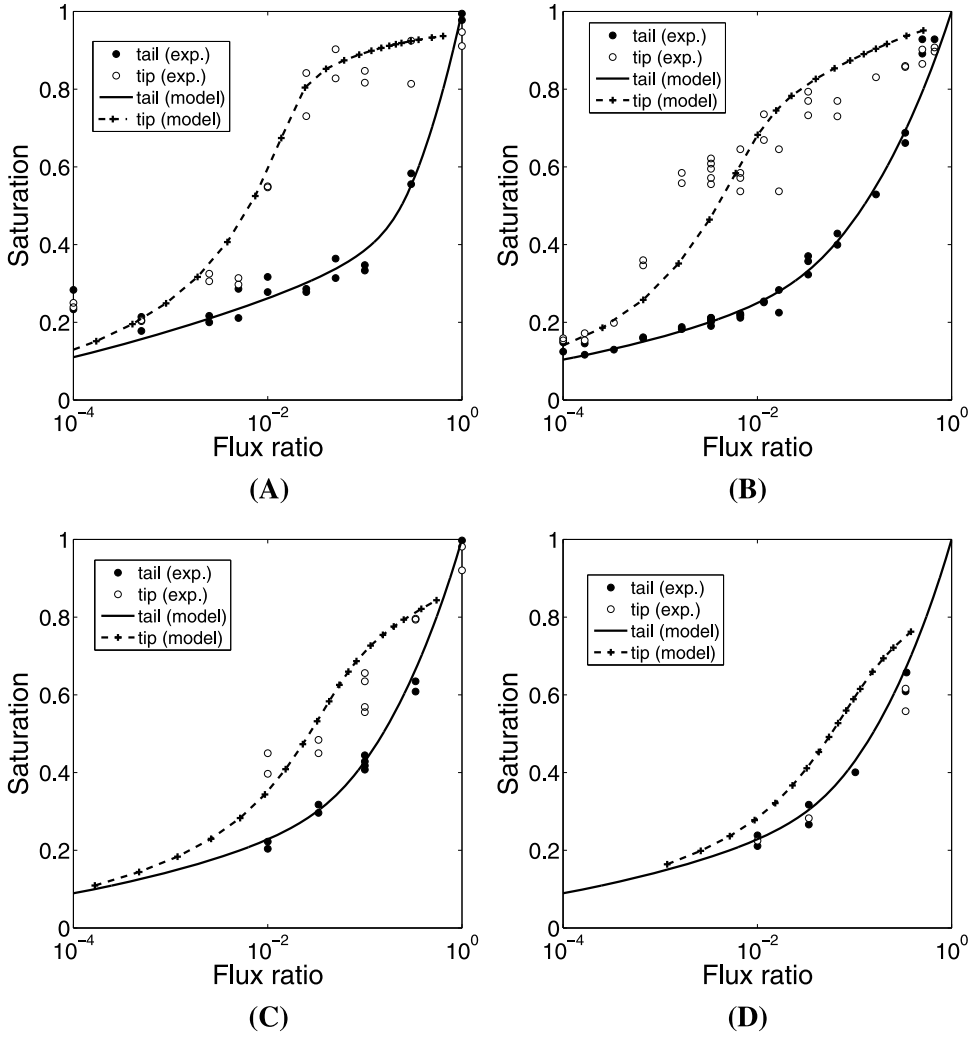

Figure 12. Comparison of the saturation overshoot predictions from our model with the quasi-1-D experiments of *DiCarlo* [2004]: (a) 30/40 dry sand, $S_0 = 0.01$, (b) 20/30 dry sand, $S_0 = 0.01$, (c) 20/30 sand, $S_0 = 0.03$, and (d) 20/30 sand, $S_0 = 0.06$.

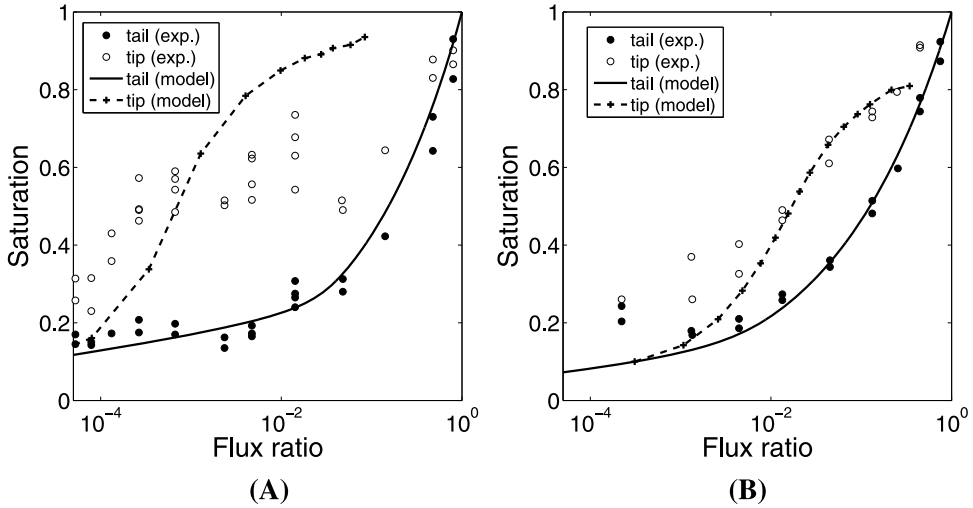

Figure 13. Comparison of the saturation overshoot predictions from our model with the quasi-1-D experiments of *DiCarlo* [2004]: (a) 12/20 dry sand and (b) grey sand.

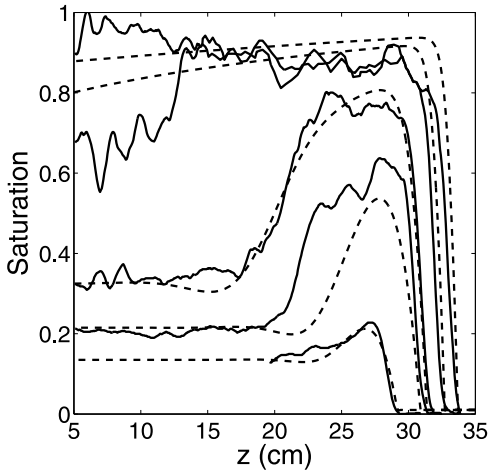

Figure 14. Simulated saturation profiles for the 20/30 dry sand with different flux ratios (dashed lines) and comparison with the experimental measurements of *DiCarlo* [2004] (solid lines). We set a gravity number of $Gr = 1/3$. The reference length is 1 cm, and therefore we are assuming a capillary rise of 3 cm.

is very efficient for spectral discretizations. We acknowledge that the wetting front is not fully resolved in our simulations, and therefore the full extent of the saturation overshoots at the finger tips is not converged in the computations presented here. From simulations on coarser grids, finger width and the range of finger velocities are not greatly affected. However, simulations with a finer grid will lead to a sharper wetting front and larger saturation overshoot at the finger tips.

[73] Snapshots of the saturation field corresponding to the two permeability fields are shown in Figure 15. The most significant feature of the simulated saturation field is the development and growth of gravity fingers that follow the pattern observed in visual laboratory experiments (compare Figures 15b and 15d with, e.g., *Glass et al.* [1989b] and *Selker et al.* [1992b]). Our model also predicts the observed saturation overshoot at the tip of the fingers, and the existence of a saturation ridge along the finger root front (also known as distribution layer), which should be analyzed in future experiments.

[74] In Figure 16, we show eight snapshots with the evolution of the fingered flow for the case with finger-scale correlation length heterogeneity. This sequence illustrates the process of finger formation from the initial condition, and finger persistence once the fingers form: finger width is constant along the length of the finger, and also essentially constant in time. The presence of mild heterogeneity induces slight meandering of the fingers, which show "slabs" of alternate high and low saturation. Their predominant straight shape is, however, preserved. Compared to the case of a homogeneous system, heterogeneity also results in a wider distribution of finger velocities.

[75] Additional insight into the behavior of the system is obtained by analyzing the capillary pressure term and the fourth-order term, which contribute, along with gravity, to

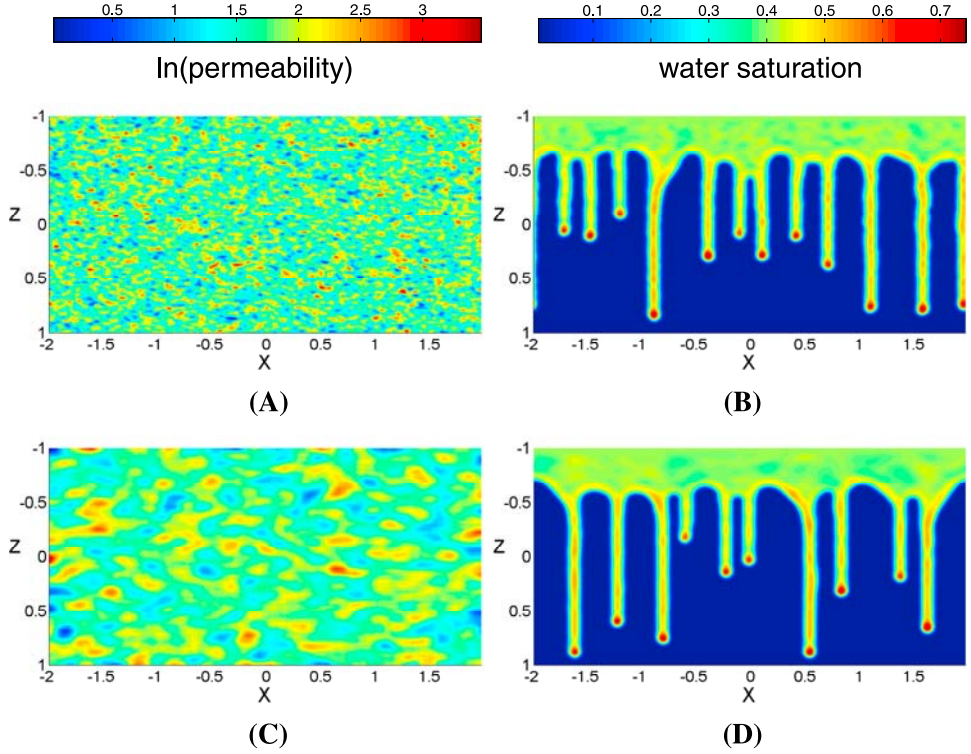

Figure 15. Two-dimensional simulations of wetting front instability in heterogeneous media. (a) Natural logarithm of the permeability field for the case with short correlation length. (b) Corresponding saturation field at $t = 174$. (c) Natural logarithm of the permeability field for the case with finger-scale correlation length. (d) Corresponding saturation field at $t = 174$.

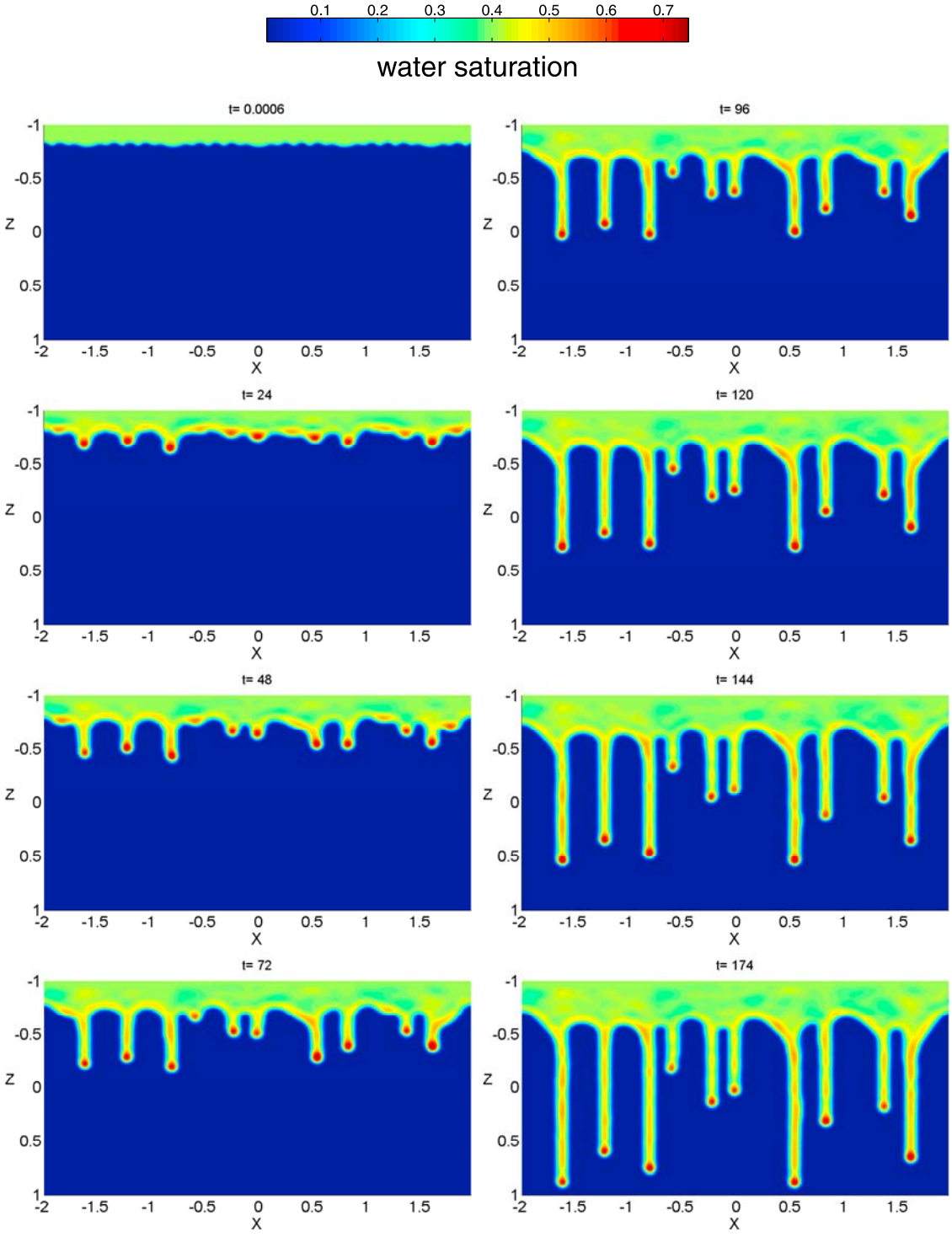

Figure 16. Two-dimensional simulations of fingered flow for the case with finger-scale correlation length heterogeneity (Figure 15d). Shown are the snapshots at different simulation times, illustrating the details of the initial condition, finger formation at early time, and finger persistence at late time.

the flow potential (see equation (12)). In Figure 17 we plot the dimensionless capillary pressure head, $Gr^{-1}J(S)$, and the dimensionless fourth-order term, $Gr^{-3}\nabla^2 S$, for the case with finger-scale correlation length heterogeneity at $t = 174$ (Figure 15d).

[76] The distribution of capillary pressure reflects the fingered pattern. Average horizontal gradients of capillary pressure between the finger core and the space between fingers are of the order of $Gr^{-1}\delta J/\delta x \approx 0.2$. Although we have not made any attempt to reproduce them quantitatively, horizontal matric potential gradients of this magnitude are observed in the experiments of *Selker et al.* [1992a]. Figure 17b shows the contribution to the potential from the fourth-order term. This term takes highest values on a fringe immediately outside of the fingered wetting front, where the saturation field is "convex," and lowest values along

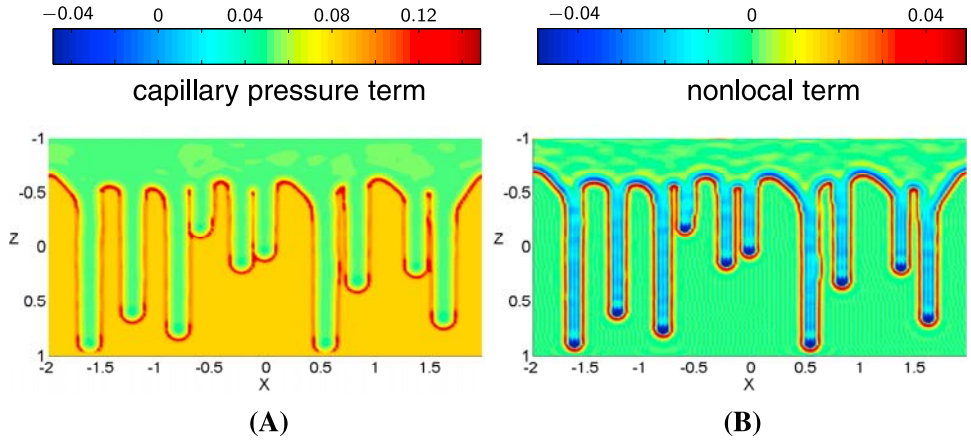

Figure 17. (a) Dimensionless capillary pressure head, $Gr^{-1}J(S)$, and (b) dimensionless nonlocal term, $Gr^{-3}\nabla^2 S$, for the case with finger-scale correlation length heterogeneity at t = 174 (Figure 15d). The distribution of capillary pressure reflects the fingered pattern. The nonlocal term takes highest values on a fringe immediately outside of the fingered wetting front, where the saturation field is convex.

the finger core and, especially, at the finger tip, where the saturation field is "concave." The flow induced by this term is toward the fringe of high values, which explains finger persistence without hysteresis effects, and the interpretation of this fourth-order term as an effective surface tension along the wetting front.

[77] When we compute the average saturation $\overline{S}$ as a function of depth, we obtain a rather dispersed infiltration profile (Figure 18a). The solution is completely different from the compact front that would be predicted from the one-dimensional Richards equation. The average saturation is approximately self-similar: the saturation profiles at different times collapse onto a single curve $\overline{S}$ (ξ) under the scaling $\xi = z/t$ (Figure 18b).

[78] A critical aspect of the impact of fingering on transport mechanisms is the relative velocities of the fingers with respect to the root front they emerge from. The larger the ratio of finger/root velocities, the more relevant fingering is; this ratio is indicative of the fraction of the flow that is channelized through the fingers. The key parameters governing finger-to-root velocity ratio are the initial saturation and the form of the relative permeability function. As an example, we repeat the simulation for the permeability field in Figure 15c, but now with different relative permeability functions. We analyze the role of the power law exponent in the range of small water saturations. In particular, we compare simulation results obtained with $k_r = S^5$ (Figure 19a) and $k_r = S^3$ (Figure 19b). It is apparent that the fingering instability becomes much milder as the power law exponent decreases. This behavior is consistent with the dependence of the saturation overshoot on the relative permeability exponent, hinting at a direct relation between

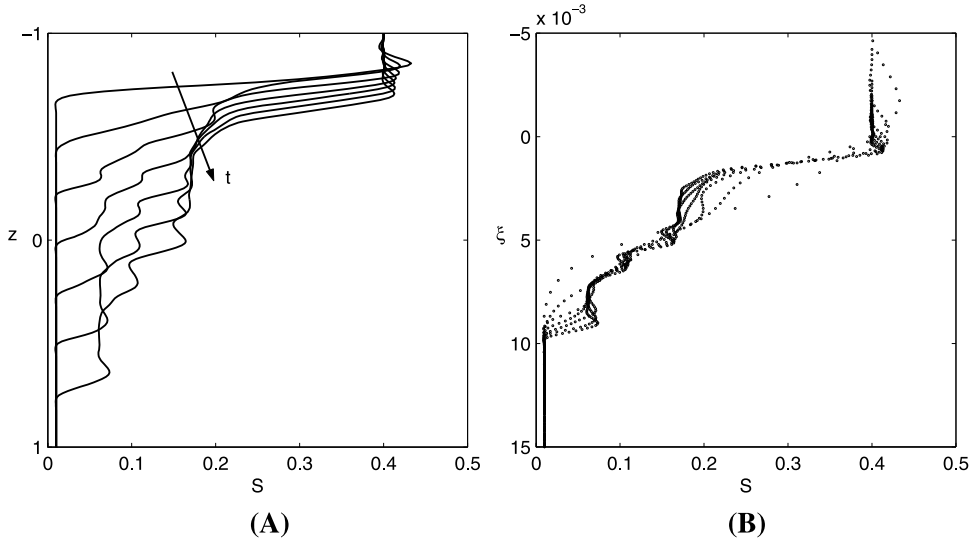

Figure 18. (a) Evolution of the average saturation as a function of depth for the 2-D simulation with short correlation length. The saturation profile is completely different from what would be predicted by a 1-D simulation of Richards' equation. (b) Average saturation, at different simulation times, as a function of the similarity variable $\xi = z/t$. The curves at different times collapse onto each other, suggesting that the infiltration process is self-similar.

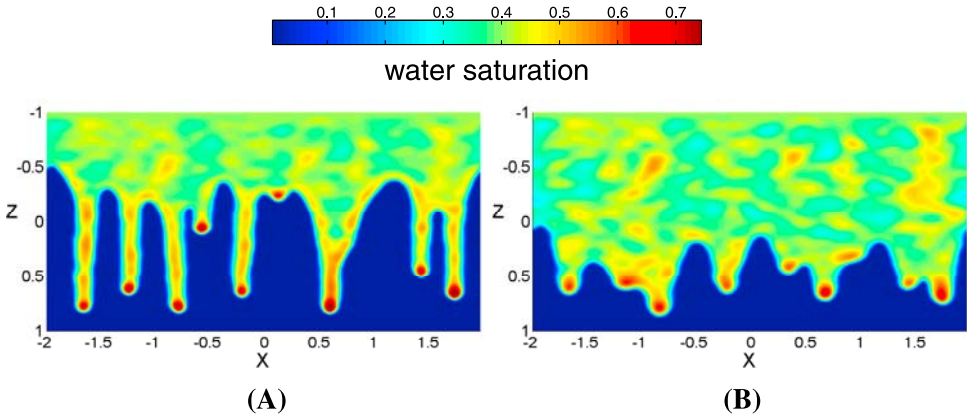

Figure 19. Two-dimensional simulations of wetting front instability in heterogeneous media. Influence of the nonlinearity of the relative permeability. (a) Saturation map for $k_r = S^5$ at $t = 7.2$. (b) Saturation map for $k_r = S^3$ at $t = 1.56$.

saturation overshoot and gravity fingering. This link is explored next.

7. Saturation Overshoot and the Onset of Fingering

[79] It has been hypothesized that saturation overshoot at the wetting front is the mechanism responsible for the formation of gravity fingers during infiltration [*Geiger and Durnford*, 2000; *Eliassi and Glass*, 2001; *Egorov et al.*, 2003]. Experimental evidence seemed to confirm these intuitions [*DiCarlo*, 2004]. The link between saturation overshoot and instability, by means of a linear stability analysis, has been investigated by *Nieber et al.* [2005] for an extended model with a relaxation dynamic term. They showed that the magnitude of the instability is related to the magnitude of the overshoot. For a very slight overshoot the flow is still basically stable; once past a critical value the flow becomes unstable.

[80] Here, we show that such a relationship between overshoot and instability of the wetting front can be naturally understood within the proposed theory. We establish the link between saturation overshoot and finger formation by performing a linear stability analysis of our model [*Cueto-Felgueroso and Juanes*, 2009b]. Stability refers here to the growth or decay of planar infinitesimal perturbations to the traveling wave solutions to equation (23). For a given set of parameters (gravity number, initial saturation, flux ratio, and constitutive relations) we compute the dispersion relation: a curve of the asymptotic growth factor β associated with each frequency ω of the initial perturbation. A positive value of β indicates asymptotic exponential growth of the perturbation. Negative values are indicative of asymptotic exponential decay. From the dispersion curve, we determine the frequency $\omega_{\max}$ of the most unstable mode, as well as its associated asymptotic growth factor $\beta_{\max}$.

[81] The dependency of the stability properties on the various parameters is shown in Figure 20. The growth factor and frequency of the most unstable mode both increase linearly with the gravity number Gr (Figure 20a). This reflects the stabilizing effect of capillary diffusion. From the perspective of characterizing the incipient fingers, this can be interpreted as the formation of thicker, slower fingers as $Gr \to 0$. For a fixed gravity number, capillary effects are smaller for higher values of the Brooks-Corey parameter λ (recall equation (26)). As a result, $\beta_{\max}$ increases with increasing λ. The most unstable mode, however, is rather insensitive to λ (Figure 20b). Consistent with experimental observations, the initial water saturation has a critical effect on the instability: even small values of S_0 result in a drastic reduction of $\beta_{\max}$, effectively suppressing the instability (Figure 20c). Of particular importance is the dependence of asymptotic exponential growth on the flux ratio R_s. For very low values of R_s, the corresponding value of $\beta_{\max}$ is also very small. Then, the growth rate increases with increasing values of R_s, while the frequency of the most unstable mode remains fairly constant. One of the key results of the stability analysis is that there is a critical flux ratio beyond which $\beta_{\max}$ starts to decrease, along with a decrease in $\omega_{\max}$. This trend means that for a sufficiently large flux ratio, close to saturated conditions, the instability is suppressed (Figure 20d).

[82] We now analyze the relation between saturation overshoot and flow instability. We compute traveling wave solutions to equation (23) for increasing flux ratios $R_s \in [0, 1]$. Through a linear stability analysis [*Cueto-Felgueroso and Juanes*, 2009b], we determine the maximum growth factor $\beta_{\max}$ and the corresponding wave number $\omega_{\max}$ of the perturbation. We adopt $Gr = 1$, $S_0 = 0.01$ and the constitutive relations

$$k_r(S) = S^3, \qquad J(S) = S^{-1/5}. \tag{33}$$

The compressibility parameter is $\kappa = 100$.

[83] Sample traveling waves for different flux ratios are shown in Figure 21a. As the flux ratio increases, the overshoot at the tip also increases. Eventually, the tip saturates and the traveling waves exhibit a relatively flat plateau near the wetting front. Figure 21b shows the "instability path" in $\beta_{\max} - \omega_{\max}$ space, for increasing flux ratios between 0 and 1. Initially, as the flux ratio increases, the system becomes more unstable but with a relatively constant unstable frequency. Beyond a critical flux ratio,

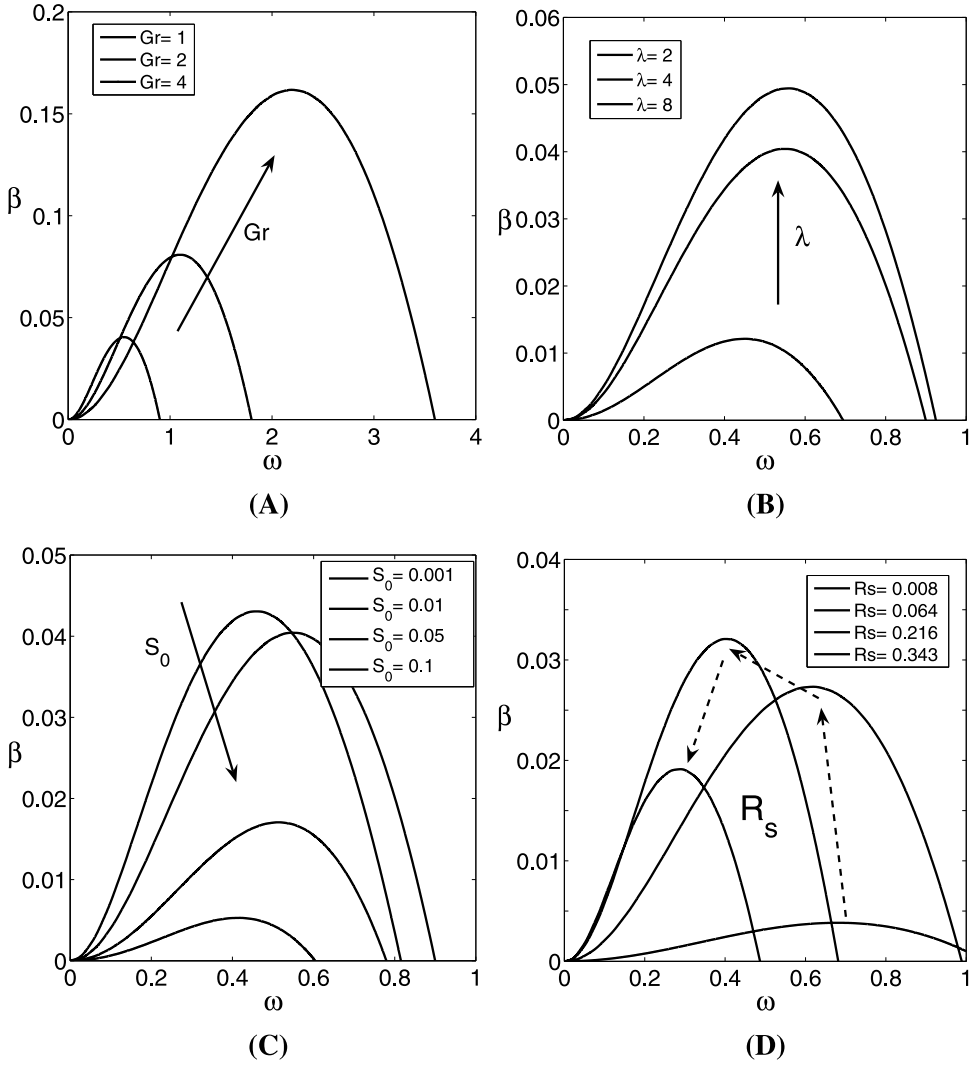

Figure 20. Influence of the model parameters on the stability properties of the traveling wave solutions to equation (23). These results correspond to the traveling waves in Figure 7. (a) Influence of the gravity number *Gr*. (b) Influence of the Brooks-Corey parameter λ. (c) Influence of the initial water saturation S_0. (d) Influence of the flux ratio $R_s = k_r(S_-)$.

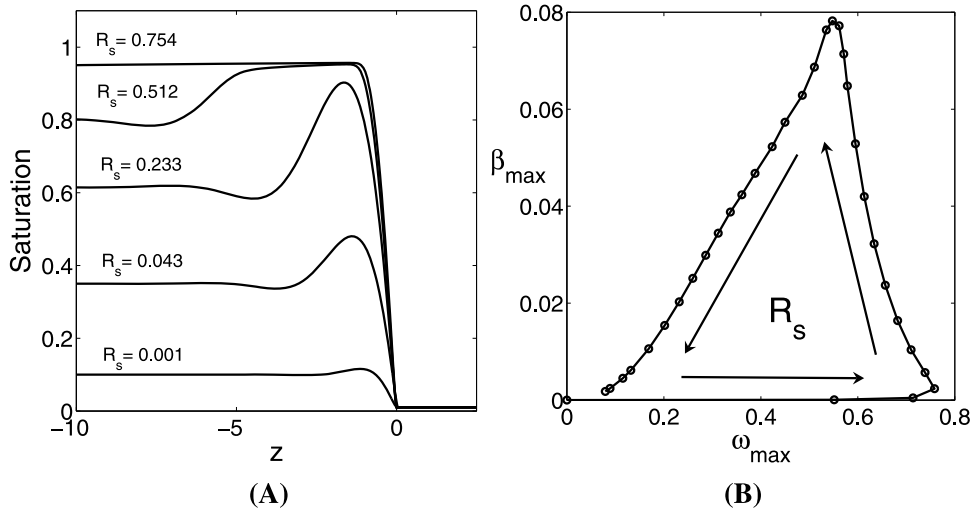

Figure 21. Relationship between saturation overshoot and stability. (a) Sample traveling waves for various flux ratios. (b) Locus of the pairs (ω_{max}, β_{max}), for the range $R_s \in [0, 0.925]$.

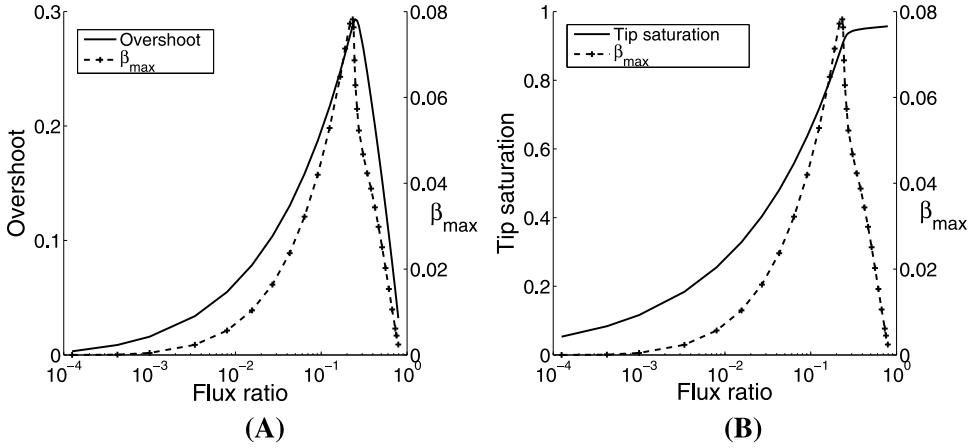

Figure 22. Relationship between saturation overshoot and stability. (a) Curves of the saturation overshoot and the maximum growth rate β_{max} as a function of flux ratio. The two curves are essentially coincident, strongly supporting the hypothesis that water pileup is the mechanism responsible for wetting front instability. (b) Curves of the saturation at the tip and the maximum growth rate β_{max} as a function of flux ratio. The instability decreases sharply for fully saturated conditions.

however, there is a transition back to stability, in the form of slower (decreasing β_{max}), thicker fingers (decreasing ω_{max}).

[84] A powerful, quantitative analysis of this general picture is provided by Figure 22a. We plot the saturation overshoot and maximum growth factor β_{max}, against flux ratio. The two curves are essentially on top of each other, strongly suggesting a direct relation between the magnitude of the pileup effect and the instability of the front. Both the saturation overshoot and β_{max} are monotonically increasing functions of the flux ratio, until the tip saturates (Figure 22b). After saturation, β_{max} shows a fast decay, and eventually the system is stable for $R_s = 1$. Near-saturated conditions lead to more stable fronts than unsaturated flows.

8. Conclusions and Outlook

[85] We have presented a phase field model of infiltration that explains gravity fingering during water infiltration in soil [*Cueto-Felgueroso and Juanes*, 2008]. The model is an extension of the traditional Richards equation, and it introduces a new term, a fourth-order derivative in space, but not a new parameter. We propose a scaling that links the magnitude of the new term to the relative strength of gravity-to-capillary forces already present in Richards' equation. We motivated the new model by analogy with the thin-film equations, which describe a similar phenomenon: the instability of a liquid film down a plane. The model is formulated, however, in the framework of phase field models. This allowed us to endow the model with a sound thermodynamical basis, and to refine it to constrain the saturation field between its physical values (0 and 1).

[86] The comparison with experiments is very favorable. In 1-D, the model reproduces the trends of saturation overshoot versus infiltration rate observed experimentally for different sands and different initial saturations. It also reproduces the saturation profile behind the wetting front. In 2-D, numerical simulations show the formation of gravity fingers with the appearance and characteristics (finger width, finger velocity, and oversaturation at the tip) observed in the experiments [*Cueto-Felgueroso and Juanes*, 2008]. Our simulations also show the pervasive nature of the fingers, even in the presence of heterogeneity, and they elucidate the critical role of the initial saturation and the nonlinearity of the unsaturated conductivity in the development of the fingering instability.

[87] The linear stability analysis of the model [*Cueto-Felgueroso and Juanes*, 2009b, 2009a] allowed us to establish a direct relationship between the saturation overshoot and the strength of the wetting front instability, supporting the view that saturation overshoot is a prerequisite for gravity fingering [*Geiger and Durnford*, 2000; *Eliassi and Glass*, 2001; *Nieber et al.*, 2005].

[88] It may seem counterintuitive that by adding a highly dissipative fourth-order derivative to a model that is totally stable, Richards' equation, a conditionally stable model emerges. The physical explanation is that the fourth-order term introduces a macroscopic surface tension at the wetting front, responsible for a hold-back–pileup effect [*Eliassi and Glass*, 2002]. The model predicts an accumulation of water at the front, which then has sufficient "energy" to trigger the instability.

[89] The phase field model of unsaturated flow presented here is a first step toward the explanation and quantitative prediction of the dynamics of unstable multiphase flow through porous media using continuum models.

[90] **Acknowledgments.** We thank John Selker for leading an insightful review process, which led to an improved presentation of the material. We gratefully acknowledge funding for this research, provided by Eni S.p.A. under the Multiscale Reservoir Science project and by the ARCO Chair in Energy Studies.

References

Aker, E., K. J. Måløy, A. Hansen, and G. G. Batrouni (1998), A two-dimensional network simulator for two-phase flow in porous media, *Transp. Porous Media*, *32*, 163–186.

Alava, M., M. Dubé, and M. Rost (2004), Imbibition in disordered media, *Adv. Phys.*, *53*, 83–175.

Allison, G. B., G. W. Gee, and S. W. Tyler (1994), Vadose-zone techniques for estimating groundwater recharge in arid and semiarid regions, *Soil Sci. Soc. Am. J.*, *58*, 6–14.

Auradou, H., K. J. Måløy, J. Schmittbuhl, A. Hansen, and D. Bideau (1999), Competition between correlated buoyancy and uncorrelated capillary effects during drainage, *Phys. Rev. E*, *60*, 7224–7234.

Avraam, D. G., and A. C. Payatakes (1995), Flow regimes and relative permeabilities during steady-state 2-phase flow in porous-media, *J. Fluid Mech.*, *293*, 207–236.

Bauters, T. W. J., D. A. DiCarlo, T. S. Steenhuis, and J.-Y. Parlange (1998), Preferential flow in water-repellent sands, *Soil Sci. Soc. Am. J.*, *62*, 1185–1190.

Bauters, T. W. J., D. A. DiCarlo, T. S. Steenhuis, and J.-Y. Parlange (2000), Soil water content dependent wetting front characteristics in sands, *J. Hydrol.*, *231*, 244–254.

Bear, J. (1972), *Dynamics of Fluids in Porous Media*, rev. ed., Elsevier, New York.

Beliaev, A. Y., and S. M. Hassanizadeh (2001), A theoretical model of hysteresis and dynamic effects in the capillary relation for two-phase flow in porous media, *Transp. Porous Media*, *43*, 487–510.

Berkowitz, B., and R. P. Ewing (1998), Percolation theory and network modeling applications in soil physics, *Surv. Geophys.*, *19*, 23–72.

Bertozzi, A. L., and M. P. Brenner (1997), Linear stability and transient growth in driven contact lines, *Phys. Fluids*, *9*, 530–539.

Birovljev, A., L. Furuberg, J. Feder, T. Jøssang, K. J. Måløy, and A. Aharony (1991), Gravity invasion percolation in two dimensions: Experiment and simulation, *Phys. Rev. Lett.*, *67*, 584–587.

Blunt, M., M. J. King, and H. Scher (1992), Simulation and theory of two-phase flow in porous media, *Phys. Rev. A*, *46*, 7680–7699.

Boettinger, W. J., J. A. Warren, C. Beckermann, and A. Karma (2002), Phase-field simulation of solidification, *Annu. Rev. Mater. Res.*, *32*, 163–194.

Bray, A. J. (1994), Theory of phase-ordering kinetics, *Adv. Phys.*, *43*, 357–459.

Brooks, R. H., and A. T. Corey (1966), Properties of porous media affecting fluid flow, *J. Irrig. Drain. Div.*, *IR2*, 61–88.

Buckingham, R. (1907), Studies on the movement of soil moisture, *Bull. 38*, pp. 29–61, Bur. of Soils, Dep. of Agric., Washington, D. C.

Buldyrev, S. V., A.-L. Barabasi, F. Caserta, S. Havlin, H. E. Stanley, and T. Vicsek (1992), Anomalous interface roughening in porous media: Experiment and model, *Phys. Rev. A*, *45*, R8313–R8316.

Cahn, J. W. (1961), On spinoidal decomposition, *Acta Metall.*, *9*, 795–801.

Cahn, J. W., and J. E. Hilliard (1958), Free energy of non-uniform systems. I. Interfacial free energy, *J. Chem. Phys.*, *28*, 258–267.

Cattaneo, C. (1958), A form of heat conduction equation which eliminates the paradox of instantaneous propagation, *C. R. Hebd. Seances Acad. Sci.*, *247*, 431–433.

Chuoke, R. L., P. van Meurs, and C. van der Poel (1959), The instability of slow, immiscible, viscous liquid-liquid displacements in permeable media, *Trans. Am. Inst. Min. Metall. Pet. Eng.*, *216*, 188–194.

Compte, A., and R. Metzler (1997), The generalized Cattaneo equation for the description of anomalous transport processes, *J. Phys. A Math. Gen.*, *30*, 7277–7289.

Cuesta, C., and J. Hulshof (2003), A model problem for groundwater flow with dynamic capillary pressure: Stability of traveling waves, *Nonlinear Anal.*, *52*, 1199–1218.

Cuesta, C., C. J. van Duijn, and J. Hulshof (2000), Infiltration in porous media with dynamic capillary pressure: Travelling waves, *Eur. J. Appl. Math.*, *11*, 381–397.

Cueto-Felgueroso, L., and R. Juanes (2008), Nonlocal interface dynamics and pattern formation in gravity-driven unsaturated flow through porous media, *Phys. Rev. Lett.*, *101*, 244504, doi:10.1103/PhysRevLett.101.244504.

Cueto-Felgueroso, L., and R. Juanes (2009a), Adaptive rational spectral methods for the linear stability analysis of nonlinear fourth-order problems, *J. Comput. Phys.*, *228*, 6536–6552, doi:10.1016/j.jcp.2009.05.045.

Cueto-Felgueroso, L., and R. Juanes (2009b), Stability analysis of a phase-field model of gravity-driven unsaturated flow through porous media, *Phys. Rev. E*, *79*, 036301, doi:10.1103/PhysRevE.79.036301.

Cueto-Felgueroso, L., and J. Peraire (2008), A time-adaptive finite volume method for the Cahn-Hilliard and Kuramoto-Sivashinsky equations, *J. Comput. Phys.*, *227*, 9,985–10,017.

Dahle, H. K., and M. A. Celia (1999), A dynamic network model for two-phase immiscible flow, *Comput. Geosci.*, *3*, 1–22.

Dahle, H. K., M. A. Celia, and S. M. Hassanizadeh (2005), Bundle-of-tubes model for calculating dynamic effects in the capillary-pressure-saturation relationship, *Transp. Porous Media*, *58*, 5–22.

de Gennes, P. G. (1985), Wetting: Statics and dynamics, *Rev. Mod. Phys.*, *57*, 827–863.

del Rio, J. A., and M. L. de Haro (1991), A generalization of the Richards equation within extended irreversible thermodynamics, *Water Resour. Res.*, *27*, 2141–2142.

DiCarlo, D. A. (2004), Experimental measurements of saturation overshoot on infiltration, *Water Resour. Res.*, *40*, W04215, doi:10.1029/2003WR002670.

DiCarlo, D. A. (2005), Modeling observed saturation overshoot with continuum additions to standard unsaturated theory, *Adv. Water Resour.*, *28*, 1021–1027.

DiCarlo, D. A. (2007), Capillary pressure overshoot as a function of imbibition flux and initial water content, *Water Resour. Res.*, *43*, W08402, doi:10.1029/2006WR005550.

DiCarlo, D. A., and M. J. Blunt (2000), Determination of finger shape using the dynamic capillary pressure, *Water Resour. Res.*, *36*, 2781–2785.

DiCarlo, D. A., R. Juanes, T. LaForce, and T. P. Witelski (2008), Nonmonotonic traveling wave solutions of infiltration in porous media, *Water Resour. Res.*, *44*, W02406, doi:10.1029/2007WR005975.

Diment, G. A., and K. K. Watson (1983), Stability analysis of water movement in unsaturated porous materials: 2. Numerical studies, *Water Resour. Res.*, *19*, 1002–1010.

Diment, G. A., and K. K. Watson (1985), Stability analysis of water movement in unsaturated porous materials: 3. Experimental studies, *Water Resour. Res.*, *21*, 979–984.

Diment, G. A., K. K. Watson, and P. J. Blennerhassett (1982), Stability analysis of water movement in unsaturated porous materials: 1. Theoretical considerations, *Water Resour. Res.*, *18*, 1248–1254.

Domenico, P. A., and F. W. Schwartz (1998), *Physical and Chemical Hydrogeology*, 2nd ed., John Wiley, New York.

Du, X., T. Yao, W. D. Stone, and J. M. H. Hendrickx (2001), Stability analysis of the unsaturated water flow equation: 1. Mathematical derivation, *Water Resour. Res.*, *37*, 1869–1874.

Dubé, M., M. Rost, K. R. Elder, M. Alava, S. Majaniemi, and T. Ala-Nissila (1999), Liquid conservation and nonlocal interface dynamics in imbibition, *Phys. Rev. Lett.*, *83*, 1628–1631.

Dubé, M., M. Rost, and M. Alava (2000a), Conserved dynamics and interface roughening in spontaneous imbibition: A critical overview, *Eur. Phys. J. B*, *15*, 691–699.

Dubé, M., M. Rost, K. R. Elder, M. Alava, S. Majaniemi, and T. Ala-Nissila (2000b), Conserved dynamics and interface roughening in spontaneous imbibition: A phase field model, *Eur. Phys. J. B*, *15*, 701–714.

Dubé, M., S. Majaniemi, M. Rost, K. R. Elder, M. Alava, and T. Ala-Nissila (2001), Interface pinning in spontaneous imbibition, *Phys. Rev. E*, *64*, 051605, doi:10.1103/PhysRevE.64.051605.

Dubé, M., C. Daneault, V. Vuorinen, M. Alava, and M. Rost (2007), Front roughening in three-dimensional imbibition, *Eur. Phys. J. B*, *56*, 15–26.

Dullien, F. A. L. (1991), *Porous Media: Fluid Transport and Pore Structure*, 2nd ed., Academic, San Diego, Calif.

Egorov, A. G., R. Z. Dautov, J. L. Nieber, and A. Y. Sheshukov (2003), Stability analysis of gravity-driven infiltrating flow, *Water Resour. Res.*, *39*(9), 1266, doi:10.1029/2002WR001886.

Elder, K. R., M. Grant, N. Provatas, and J. M. Kosterlitz (2001), Sharp interface limits of phase-field models, *Phys. Rev. E*, *64*, 21604, doi:10.1103/PhysRevE.64.021604.

Eliassi, M., and R. J. Glass (2001), On the continuum-scale modeling of gravity-driven fingers in unsaturated porous media: The inadequacy of the Richards equation with standard monotonic constitutive relations and hysteretic equations of state, *Water Resour. Res.*, *37*, 2019–2035.

Eliassi, M., and R. J. Glass (2002), On the porous-continuum modeling of gravity-driven fingers in unsaturated materials: Extension of standard theory with a hold-back-pile-up effect, *Water Resour. Res.*, *38*(11), 1234, doi:10.1029/2001WR001131.

Eliassi, M., and R. J. Glass (2003), On the porous continuum-scale modeling of gravity-driven fingers in unsaturated materials: Numerical solution of a hypodiffusive governing equation that incorporates a hold-back-pile-up effect, *Water Resour. Res.*, *39*(6), 1167, doi:10.1029/2002WR001535.

Emmerich, H. (2008), Advances of and by phase-field modelling in condensed-matter physics, *Adv. Phys.*, *57*, 1–87.

Ewing, R. P., and B. Berkowitz (1998), A generalized growth model for simulating initial migration of dense non-aqueous phase liquids, *Water Resour. Res.*, *34*, 611–622.

Ferer, M., C. Ji, G. S. Bromhal, J. Cook, G. Ahmadi, and D. H. Smith (2004), Crossover from capillary fingering to viscous fingering for immiscible unstable flow: Experiment and modeling, *Phys. Rev. E*, *70*, 016303, doi:10.1103/PhysRevE.70.016303.

Frette, V., J. Feder, T. Jøssang, and P. Meakin (1992), Buoyancy-driven fluid migration in porous media, *Phys. Rev. Lett.*, *68*, 3164–3167.

Fürst, T., R. Vodák, M. Šír, and M. Bíl (2009), On the incompatibility of Richards' equation and finger-like infiltration in unsaturated homogeneous porous media, *Water Resour. Res.*, *45*, W03408, doi:10.1029/2008WR007062.

Geiger, S. L., and D. S. Durnford (2000), Infiltration in homogeneous sands and a mechanistic model of unstable flow, *Soil Sci. Soc. Am. J.*, *64*, 460–469.

Glass, R. J., and L. Yarrington (1996), Simulation of gravity fingering in porous media using a modified invasion percolation model, *Geoderma*, *70*, 231–252.

Glass, R. J., and L. Yarrington (2003), Mechanistic modeling of fingering, nonmonotonicity, fragmentation, and pulsation within gravity/buoyant destabilized two-phase/unsaturated flow, *Water Resour. Res.*, *39*(3), 1058, doi:10.1029/2002WR001542.

Glass, R. J., J.-Y. Parlange, and T. S. Steenhuis (1989a), Wetting front instability: 1. Theoretical discussion and dimensional analysis, *Water Resour. Res.*, *25*, 1187–1194.

Glass, R. J., J.-Y. Parlange, and T. S. Steenhuis (1989b), Wetting front instability: 2. Experimental determination of relationships between system parameters and two-dimensional unstable flow field behaviour in initially dry porous media, *Water Resour. Res.*, *25*, 1195–1207.

Gollub, J. P., and J. S. Langer (1999), Pattern formation in nonequilibrium physics, *Rev. Mod. Phys.*, *71*, S396–S403.

Gomez, H., V. M. Calo, Y. Bazilevs, and T. J. R. Hughes (2008), Isogeometric analysis of the Cahn-Hilliard phase-field model, *Comput. Methods Appl. Mech. Eng.*, *197*, 4333–4352.

Green, W. H., and G. A. Ampt (1911), Studies of soil physics: 1. The flow of air and water through soils, *J. Agric. Sci.*, *4*, 1–24.

Halpin-Healy, T., and Y.-C. Zhang (1995), Kinetic roughening phenomena, stochastic growth, directed polymers and all that: Aspects of multidisciplinary statistical mechanics, *Phys. Rep.*, *254*, 215–414.

Hassanizadeh, S. M., and W. G. Gray (1990), Mechanics and thermodynamics of multiphase flow in porous media including interphase boundaries, *Adv. Water Resour.*, *13*, 169–186.

Hassanizadeh, S. M., and W. G. Gray (1993a), Toward an improved description of the physics of two-phase flow, *Adv. Water Resour.*, *16*, 53–67.

Hassanizadeh, S. M., and W. G. Gray (1993b), Thermodynamic basis of capillary pressure in porous media, *Water Resour. Res.*, *29*, 3389–3405.

Hassanizadeh, S. M., M. A. Celia, and H. K. Dahle (2002), Dynamic effects in the capillary pressure-saturation relationship and its impact on unsaturated flow, *Vadose Zone J.*, *1*, 38–57.

He, S., G. L. M. K. S. Kahanda, and P. Wong (1992), Roughness of wetting fluid invasion fronts in porous media, *Phys. Rev. Lett.*, *69*, 3731–3734.

Helmig, R., A. Weiss, and B. I. Wohlmuth (2007), Dynamic capillary effects in heterogeneous porous media, *Comput. Geosci.*, *11*, 261–274.

Hendrickx, J. M. H., and T. Yao (1996), Prediction of wetting front stability in dry field soils using soil and precipitation data, *Geoderma*, *70*, 265–280.

Hernández-Machado, A., J. Soriano, A. M. Lacasta, M. A. Rodriguez, L. Ramírez-Piscina, and J. Ortín (2001), Interface roughening in Hele-Shaw flows with quenched disorder: Experimental and theoretical results, *Europhys. Lett.*, *55*, 194–200.

Hill, D. E., and J.-Y. Parlange (1972), Wetting front instability in layered soils, *Soil Sci. Soc. Am. J.*, *36*, 697–702.

Hillel, D. (1980), *Applications of Soil Physics*, Academic, San Diego, Calif.

Horton, R. E. (1933), The role of infiltration in the hydrologic cycle, *Trans. AGU*, *14*, 446–460.

Horton, R. E. (1940), An approach toward the physical interpretation of infiltration capacity, *Soil Sci. Soc. Am. Proc.*, *5*, 399–417.

Horvath, V. K., and H. E. Stanley (1995), Temporal scaling of interfaces propagating in porous media, *Phys. Rev. E*, *52*, 5166–5169.

Horvath, V. K., F. Family, and T. Vicsek (1991), Dynamic scaling of the interface in two-phase viscous flows in porous media, *J. Phys. A Math. Gen.*, *24*, L25–L29.

Huppert, H. E. (1982), Flow and instability of a viscous current down a slope, *Nature*, *300*, 427–429.

Juanes, R., E. J. Spiteri, F. M. Orr Jr., and M. J. Blunt (2006), Impact of relative permeability hysteresis on geological CO_2 storage, *Water Resour. Res.*, *42*, W12418, doi:10.1029/2005WR004806.

Kapoor, V. (1996), Criterion for instability of steady-state unsaturated flows, *Transp. Porous Media*, *25*, 313–334.

Kardar, M., G. Parisi, and Y.-C. Zhang (1986), Dynamic scaling of growing interfaces, *Phys. Rev. Lett.*, *56*, 889–892.

Karma, A., and W.-J. Rappel (1996), Numerical simulation of three-dimensional dendritic growth, *Phys. Rev. Lett.*, *77*, 4050–4053.

Kim, J. M., and S. Das Sarma (1994), Discrete models for conserved growth equations, *Phys. Rev. Lett.*, *72*, 2903–2906.

Kondic, L. (2003), Instabilities in gravity driven flow of thin fluid films, *SIAM Rev.*, *45*, 95–115.

Langer, J. S. (1989), Dendrites, viscous fingers and the theory of pattern formation, *Science*, *243*, 1150–1156.

Lee, S. H., L. Padmanabhan, and H. A. Al-Sunaidi (1996), Simulation of linear displacement experiments on massively parallel computers, *Soc. Pet. Eng. J.*, *1*, 327–340.

Lei, G. (1988), Level crossing curvature and the Laplacian, *Image Vision Comput.*, *6*, 185–188.

Lenormand, R., E. Touboul, and C. Zarcone (1988), Numerical models and experiments on immiscible displacements in porous media, *J. Fluid Mech.*, *189*, 165–187.

Leverett, M. C. (1941), Capillary behavior of porous solids, *Trans. Am. Inst. Min. Metall. Pet. Eng.*, *142*, 152–169.

Liang, X., D. P. Lettenmaier, E. F. Wood, and S. J. Burges (1994), A simple hydrologically based model of land-surface water and energy fluxes for general circulation models, *J. Geophys. Res.*, *99*, 14,415–14,428.

Liu, Y., T. S. Steenhuis, and J.-Y. Parlange (1994), Formation and persistence of fingered flow fields in coarse grained soils under different moisture contents, *J. Hydrol.*, *159*, 187–195.

Lopez, J. M. (1999), Scaling approach to calculate critical exponents in anomalous surface roughening, *Phys. Rev. Lett.*, *83*, 4594–4597.

Lowengrub, J., and L. Truskinovsky (1998), Quasi-incompressible Cahn-Hilliard fluids and topological transitions, *Proc. R. Soc. London A*, *454*, 2617–2654.

Lu, T. X., J. W. Biggar, and D. R. Nielsen (1994), Water movement in glass bead porous media: 2. Experiments of infiltration and finger flow, *Water Resour. Res.*, *30*, 3283–3290.

Manthey, S., S. M. Hassanizadeh, and R. Helmig (2005), Macro-scale dynamic effects in homogeneous and heterogeneous porous media, *Transp. Porous Media*, *58*, 5–22.

Markewitz, D., E. A. Davidson, R. Figueiredo, R. L. Victoria, and A. V. Krusche (2001), Control of cation concentrations in stream waters by surface soil processes in an Amazonian watershed, *Nature*, *410*, 802–805.

Méheust, Y., G. Løvoll, K. J. Måløy, and J. Schmittbuhl (2002), Interface scaling in a two-dimensional porous medium under combined viscous, gravity, and capillary effects, *Phys. Rev. E*, *66*, 051603, doi:10.1103/PhysRevE.66.051603.

Mirzaei, M., and D. B. Das (2006), Dynamic effects in capillary pressure-saturations relationships for two-phase flow in 3D porous media: Implications of micro-heterogeneities, *Chem. Eng. Sci.*, *62*, 1927–1947.

Mualem, Y. (1976), A new model for predicting the hydraulic conductivity of unsaturated porous media, *Water Resour. Res.*, *12*, 513–522.

Muskat, M., and M. W. Meres (1936), The flow of heterogeneous fluids through porous media, *Physics*, *7*, 346–363.

Muskat, M., R. D. Wyckoff, H. G. Botset, and M. W. Meres (1937), Flow of gas-liquid mixtures through sands, *Trans. Am. Inst. Min. Metall. Pet. Eng.*, *123*, 69–96.

Nieber, J., A. Sheshukov, A. Egorov, and R. Dautov (2003), Non-equilibrium model for gravity-driven fingering in water repellent soils: Formulation and 2D simulations, in *Soil Water Repellency: Occurrence, Consequences and Amelioration*, edited by C. J. Ritsema and L. Dekker, pp. 243–257, Elsevier, New York.

Nieber, J. L., R. Z. Dautov, A. G. Egorov, and A. Y. Sheshukov (2005), Dynamic capillary pressure mechanism for instability in gravity-driven flows: Review and extension to very dry conditions, *Transp. Porous Media*, *58*, 147–172.

O'Carroll, D. M., T. J. Phelan, and L. M. Abriola (2005), Exploring dynamic effects in capillary pressure in multistep outflow experiments, *Water Resour. Res.*, *41*, W11419, doi:10.1029/2005WR004010.

Onody, R. N., A. N. D. Posadas, and S. Crestana (1995), Experimental studies of the fingering phenomena in two dimensions and simulation using a modified percolation model, *J. Appl. Phys.*, *78*, 2970–2976.

Papatzacos, P. (2002), Macroscopic two-phase flow in porous media assuming the diffuse-interface model at pore level, *Transp. Porous Media*, *49*, 139–174.

Papatzacos, P., and S. M. Skjæveland (2004), Relative permeability from thermodynamics, *Soc. Pet. Eng. J.*, *9*, 47–56.

Papatzacos, P., and S. M. Skjæveland (2006), Diffuse-interface modeling of two-phase flow for a one-component fluid in a porous medium, *Transp. Porous Media*, *65*, 213–236.

Parlange, J.-Y., and D. E. Hill (1976), Theoretical analysis of wetting front instability in soils, *Soil Sci.*, *122*, 236–239.

Philip, J. R. (1957), The theory of infiltration: 4. Sorptivity and algebraic infiltration equations, *Soil Sci.*, *84*, 257–264.

Philip, J. R. (1969), Theory of infiltration, in *Advances in Hydroscience*, edited by V. T. Chow, pp. 215–296, Academic, New York.

Philip, J. R. (1975), Stability analysis of infiltration, *Soil Sci. Soc. Am. J.*, *39*, 1042–1049.

Porporato, A., E. Daly, and I. Rodriguez-Iturbe (2004), Soil water balance and ecosystem response to climate change, *Am. Nat.*, *164*, 625–632.

Raats, P. A. C. (1973), Unstable wetting fronts in uniform and nonuniform soils, *Soil Sci. Soc. Am. J.*, *37*, 681–685.

Richards, L. A. (1931), Capillary conduction of liquids through porous mediums, *Physics*, *1*, 318–333.

Rodriguez-Iturbe, I., P. D'Odorico, A. Porporato, and L. Ridolfi (1999), On the spatial and temporal links between vegetation, climate, and soil moisture, *Water Resour. Res.*, *35*, 3709–3722.

Saffman, P. G., and G. I. Taylor (1958), The penetration of a fluid into a porous medium or Hele-Shaw cell containing a more viscous liquid, *Proc. R. Soc. London A*, *245*, 312–329.

Sander, G. C., O. J. Glidewell, and J. Norbury (2008), Dynamic capillary pressure, hysteresis and gravity-driven fingering in porous media, *J. Phys. Conf. Ser.*, *138*, 012023, doi:10.1088/1742-6596/138/1/012023.

Schlesinger, W. H., J. F. Reynolds, G. L. Cunningham, L. F. Huenneke, W. M. Jarrell, R. A. Virginia, and W. G. Whitford (1990), Biological feedbacks in global desertification, *Science*, *247*, 1043–1048.

Selker, J. S., and M. H. Schroth (1998), Evaluation of hydrodynamic scaling in porous media using finger dimensions, *Water Resour. Res.*, *34*, 1935–1940.

Selker, J. S., P. Leclerq, J.-Y. Parlange, and T. Steenhuis (1992a), Fingered flow in two dimensions: 1. Measurement of matric potential, *Water Resour. Res.*, *28*, 2513–2521.

Selker, J. S., J.-Y. Parlange, and T. Steenhuis (1992b), Fingered flow in two dimensions: 2. Predicting finger moisture profile, *Water Resour. Res.*, *28*, 2523–2528.

Shiozawa, S., and H. Fujimaki (2004), Unexpected water content profiles under flux-limited one-dimensional downward infiltration in initially dry granular media, *Water Resour. Res.*, *40*, W07404, doi:10.1029/2003WR002197.

Sililo, O. T. N., and J. H. Tellam (2000), Fingering in unsaturated zone flow: A qualitative review with laboratory experiments in heterogeneous systems, *Ground Water*, *38*, 864–871.

Sophocleous, M. (2002), Interactions between groundwater and surface water: The state of the science, *Hydrogeol. J.*, *10*, 52–67.

Soriano, J., J. J. Ramasco, M. A. Rodriguez, A. Hernández-Machado, and J. Ortín (2002), Anomalous roughening of Hele-Shaw flows with quenched disorder, *Phys. Rev. Lett.*, *89*, 026102, doi:10.1103/PhysRevLett.89.026102.

Soriano, J., A. Mercier, R. Planet, A. Hernández-Machado, M. A. Rodríguez, and J. Ortín (2005), Anomalous roughening of viscous fluid fronts in spontaneous imbibition, *Phys. Rev. Lett.*, *95*, 104501, doi:10.1103/PhysRevLett.95.104501.

Spiteri, E. J., and R. Juanes (2006), Impact of relative permeability hysteresis on the numerical simulation of WAG injection, *J. Pet. Sci. Eng.*, *50*, 115–139.

Stauffer, F. (1978), Time dependence of the relations between capillary pressure, water content and conductivity during drainage of porous media, paper presented at IAHR Symposium on Scale Effects in Porous Media, Thessaloniki, Greece.

Stonestrom, D. A., and K. C. Akstin (1994), Nonmonotonic matric pressure histories during constant flux infiltration into homogeneous profiles, *Water Resour. Res.*, *30*, 81–91.

Sun, T., H. Guo, and M. Grant (1989), Dynamics of driven interfaces with a conservation law, *Phys. Rev. A*, *40*, 6763–6766.

Tee, T. W., and L. N. Trefethen (2006), A rational spectral collocation method with adaptively transformed Chebyshev grid points, *SIAM J. Sci. Comput.*, *28*, 1798–1811.

Torn, M. S., S. E. Trumbore, O. A. Charwick, P. M. Vitousek, and D. M. Hendricks (1997), Mineral control of soil organic carbon storage and turnover, *Nature*, *389*, 170–173.

Ursino, N. (2000), Linear stability analysis of infiltration, analytical and numerical solution, *Transp. Porous Media*, *38*, 261–271.

Valavanides, M. S., G. N. Constantinides, and A. C. Payatakes (1998), Mechanistic model of steady-state two-phase flow in porous media based on ganglion dynamics, *Transp. Porous Media*, *30*, 267–299.

Valvatne, P. H., and M. J. Blunt (2004), Predictive pore-scale modeling of two-phase flow in mixed wet media, *Water Resour. Res.*, *40*, W07406, doi:10.1029/2003WR002627.

van Duijn, C. J., G. J. M. Pieters, and P. A. C. Raats (2004), Steady flows in unsaturated soils are stable, *Transp. Porous Media*, *57*, 215–244.

van Genuchten, M. T. (1980), A closed-form equation for predicting the hydraulic conductivity of unsaturated soils, *Soil Sci. Soc. Am. J.*, *44*, 892–898.

Wang, Z., W. A. Jury, A. Tuli, and D.-J. Kim (2004), Unstable flow during redistribution: Controlling factors and practical implications, *Vadose Zone J.*, *3*, 549–559.

Weatherburn, C. E. (1927), *Differential Geometry in Three Dimensions*. vol. I, Cambridge Univ. Press, Cambridge, U. K.

Weitz, D. A., J. P. Stokes, R. C. Ball, and A. P. Kushnick (1987), Dynamic capillary pressure in porous media: Origin of the viscous fingering lengthscale, *Phys. Rev. Lett.*, *59*, 2967–2970.

Witelski, T. P. (1996), The structure of internal layers for unstable nonlinear diffusion equations, *Stud. Appl. Math.*, *97*, 277–300.

Yao, T., and J. M. H. Hendrickx (2001), Stability analysis of the unsaturated water flow equation: 2. Experimental verification, *Water Resour. Res.*, *37*, 1875–1881.

Yortsos, Y. C., B. Xu, and D. Salin (1997), Phase diagram of fully-developed drainage in porous media, *Phys. Rev. Lett.*, *79*, 4581–4584.

Zhang, Y., M. Shariati, and Y. C. Yortsos (2000), The spreading of immiscible fluids in porous media under the influence of gravity, *Transp. Porous Media*, *38*, 117–140.

Zhu, J., L.-Q. Chen, J. Shen, and V. Tikare (1999), Coarsening kinetics from a variable-mobility Cahn-Hilliard equation: Application of a semi-implicit Fourier spectral method, *Phys. Rev. E*, *60*, 3564–3572.

L. Cueto-Felgueroso and R. Juanes (corresponding author), Department of Civil and Environmental Engineering, Massachusetts Institute of Technology, Cambridge, MA 02139, USA. (lcueto@mit.edu; juanes@mit.edu)